

Meta-validation of bipartite network projections

Giulio Cimini^{1,2,*}, Alessandro Carra³, Luca Didomenicantonio³, and Andrea Zaccaria^{4,2}

¹Physics Department and INFN, University of Rome Tor Vergata, 00133 Rome (Italy)

²Enrico Fermi Research Center, 00184 Rome (Italy)

³Physics Department, Sapienza University of Rome, 00185 Rome (Italy)

⁴Institute for Complex Systems (CNR) UoS Sapienza, 00185 Rome (Italy)

*giulio.cimini@roma2.infn.it

ABSTRACT

Monopartite projections of bipartite networks are useful tools for modeling indirect interactions in complex systems. The standard approach to identify significant links is statistical validation using a suitable null network model, such as the popular configuration model (CM) that constrains node degrees and randomizes everything else. However different CM formulations exist, depending on how the constraints are imposed and for which sets of nodes. Here we systematically investigate the application of these formulations in validating the same network, showing that they lead to different results even when the same significance threshold is used. Instead a much better agreement is obtained for the same density of validated links. We thus propose a meta-validation approach that allows to identify model-specific significance thresholds for which the signal is strongest, and at the same time to obtain results independent of the way in which the null hypothesis is formulated. We illustrate this procedure using data on scientific production of world countries.

Introduction

Networks are simplified yet effective models for a large class of natural, socio-economic and technological systems described by complex interaction patterns. Independently of the nature of the underlying interactions, the network representation allows capturing the emergent features of these systems as well as their dynamical patterns¹⁻⁵. As such, network science has gained increasing popularity in the last twenty years⁶⁻⁸.

A network is labeled as *bipartite* when its elements (the nodes) can be split in two disjoint sets, such that links can only exist between nodes of different sets⁹. Bipartite networks are the natural representation for several systems, such as: social affiliation and collaboration networks, where individuals connect to the groups they are member of^{10,11}; financial and commercial ownership networks, where entities are linked to the goods they own or consume^{12,13}; trade networks, where economies connect to the products they export^{14,15}; ecological networks, where species connect to the habitat they live in^{16,17}; biological and medical networks connecting, *e.g.*, patients and diseases^{18,19}. Mathematically speaking, a bipartite network is defined as a graph with two sets L and Γ of nodes, and a $|L| \times |\Gamma|$ matrix of connections \mathbf{M} called *bi-adjacency matrix*. The generic element of this matrix is

$$M_{i\alpha} = \begin{cases} 1 & \text{if nodes } i \in L \text{ and } \alpha \in \Gamma \text{ are connected,} \\ 0 & \text{otherwise.} \end{cases} \quad (1)$$

The number of connections or *degree* of a node $i \in L$ is then defined as $k_i = \sum_{\alpha \in \Gamma} M_{i\alpha}$, while the degree of a node $\alpha \in \Gamma$ is $\kappa_\alpha = \sum_{i \in L} M_{i\alpha}$. The total number of links in the network is $E = \sum_{i \in L} k_i = \sum_{\alpha \in \Gamma} \kappa_\alpha$.

The indirect relation between two nodes belonging to the same set of a bipartite network can be measured through their *co-occurrences* (or common neighbors), namely how many nodes of the other set they are both connected to. For instance the co-occurrences of nodes i and j of set L are given by

$$C_{ij} = \sum_{\alpha \in \Gamma} M_{i\alpha} M_{j\alpha}. \quad (2)$$

The $L \times L$ square matrix \mathbf{C} represents a monopartite network obtained as the projection of the original bipartite network onto the set L (L -projection)¹². Analogously, one can project the bipartite network onto the set Γ to obtain the co-occurrences between nodes of that set (Γ -projection).

The main problem in studying bipartite network projections is that they are often very dense and thus difficult to handle with the tools of network theory. This happens because any two nodes are connected in the projected network as soon as they have a single co-occurrence. Moreover, co-occurrences can be influenced by single node variables, thus understanding whether

they indicate an effective interdependence between nodes may be difficult. For example, nodes that have high degree in the bipartite network naturally tend to have more co-occurrences than low-degree nodes (more generally, the degree sequence of the network projection is highly dependent on the degree sequence of the two sets from the original bipartite structure²⁰). It is thus useful to extract representative links of the projected network; this can be achieved using several filtering techniques, from unconditional thresholding to Minimal Spanning Trees²¹ and Planar Maximally Filtered Graphs²². Yet in order to identify the most informative co-occurrences, the statistically-grounded approach consists in performing link validation using a null network model.

Statistical validation of network patterns is a common approach in the literature (the classical applications being motifs expression analysis^{23,24}, network backbone extraction²⁵ and community detection^{26–28}). The goal is to identify the empirical patterns that deviate from a benchmark null model, in order to ensure that those patterns are indeed a salient feature of the network and not a mere consequence of some of its other properties (given the potentially strong interdependence between structural network quantities^{29–33}). Following the prescription of information theory³⁴, the null model is thus obtained by constraining some network properties and randomizing everything else. In this way, the formulated null hypothesis is that these constraints are the only explanatory variables for the network at hand; when the null hypothesis is rejected, we can state that the observed network patterns are not a mere consequence of the imposed constraints.

Going back to our context of bipartite network projections, the statistical significance of each observed co-occurrence value $C_{ij} > 0$ can be quantified through its p-value:

$$p[C_{ij}] = 1 - \sum_{x=0}^{C_{ij}-1} \pi(x|i, j), \quad (3)$$

where $\pi(\cdot|i, j)$ is the probability distribution of the expected co-occurrences between i and j under the null model. The right-hand side of eq. (3) is the probability that i and j have no less than C_{ij} co-occurrences in the null model. This quantity can be used to build a *validated* (or filtered) projection of the original bipartite network, containing only the most significant links according to the null model. For each C_{ij} , if the p-value of eq. (3) is smaller than a significance threshold (or confidence level) p^* , the link i, j is placed on the monopartite validated network; otherwise, it is discarded. In other words, the comparison is deemed statistically significant if the observed co-occurrences are an unlikely realization of the null hypothesis according to the significance level p^* (in particular, we are interested in detecting the co-occurrences that are significantly larger than their null model expectation; significantly smaller values can be obtained in a similar fashion — see Supplementary Note 1). In this way the original amount of links is drastically reduced, and the result is a much sparser validated network with a clearer meaning.

Naturally, statistical validation has some intrinsic degrees of freedom: the choice of the null model, its specific formulation, and the value of the significance level p^* . In particular, the choice of the model is a step that should be handled with care, as a bad choice may lead to wrong conclusions about the structural and functional features of the network^{35,36}. For instance, using a (bipartite) Erdős-Rényi model³⁷, *i.e.*, a random network preserving only the density of the original bipartite graph, leads to an identical distribution $\pi(\cdot|i, j)$ for each node pair i, j and thus to an unconditional global threshold to select the most significant C_{ij} values^{38,39}. However this choice does not solve the bias problem for high degree nodes, which is very important in networks given that degree distributions are typically very broad⁴⁰. A natural way to take this aspect into account is given by the popular *configuration model* (CM)^{41–43}, which generates random networks with a given degree sequence.

In the context of bipartite networks, the first model formulation of this family was obtained by constraining the degrees of nodes in one set (say L)⁴⁴. In this case, the co-occurrences probability can be computed exactly as a hypergeometric distribution^{45,46}. Yet this model solves the degree bias only partially, since it assumes nodes of the other set (say Γ) to be equivalent and interchangeable. The alternative approach is to model random bipartite networks preserving the degrees of both node sets L and Γ , and then use these networks to obtain the null model for the projected network. *Degree sequence models* follow this approach, however they either require multiple observations of the empirical network⁴⁷ or are based on computational link swap methods⁴⁸ that are typically impractical and biased⁴⁹. An exception is represented by the recently proposed *Curveball* algorithm^{50–52}, a link swap method that is extremely efficient in generating network configurations and is ergodic (*i.e.*, it can sample uniformly over the set of all possible network configurations). The alternative route to Monte Carlo sampling is represented by maximum-entropy models. The *Bipartite Configuration Model* (BiCM)⁵³ allows generating an ensemble of bipartite networks where node degrees of both sets L and Γ are preserved as ensemble expectations. The null model for the network projections is then obtained by projecting BiCM-generated networks^{54,55}. This latter approach allows computing the co-occurrences distributions both numerically and analytically, and simplifies as a *Bipartite Partial Configuration Model* (BiPCM) when degree constraints are imposed only on one set of nodes. At last we note that, in principle, the projection of a bipartite network can be statistically validated also using a null model for monopartite weighted networks^{25,33,56}. That is, instead of defining the null model on the bipartite network and then deriving its formulation for the network projection, the null model can be directly defined on the monopartite projection. However this approach discards the information contained in the

original bipartite network, and as such typically leads to completely different and not significant outcomes (see Supplementary Note 2).

To sum up, the four main CM-based null models for bipartite network projections proposed in the literature (Hypergeometric, Curveball, BiPCM and BiCM) can differ under two aspects. The first aspect concerns which constraints are imposed, whether the degrees of one set or both sets of the bipartite network. We can thus speak of “partial” models (Hypergeometric and BiPCM) and “full” models (Curveball and BiCM). The second aspect concerns how these constraints are imposed, either exactly (hard constraints) or as ensemble expectations (soft constraints). Using the analogy with statistical physics³⁴, we can refer to these approaches respectively as “microcanonical” models (Hypergeometric and Curveball) and “canonical” models (BiPCM and BiCM). Table 1 summarizes this classification (see the Methods section for the formal definition of the four null models). A fundamental point that has not been addressed so far is whether these formulations lead to different validated networks, and thus how to interpret and compare results of the various studies in the literature.

Here we provide, for the first time to our knowledge, a systematic comparison of validation results obtained with the various CM formulations for bipartite network projections. We find that albeit based on very similar null hypothesis, the different formulations lead to very different filtered networks even for the same value of validation threshold p^* . However we show that a reconciliation of results is possible within a region of model-specific thresholds p^* such that the densities of links validated by the null models overlap. In particular we show that a common community structure may emerge in this region. This criterion provides a quantitative approach to build a meta-validated network projection that is independent on the specific implementation of the null model.

Table 1. Classification of configuration models (CM) for bipartite network projections by number and type of constraints. Partial models only constraints the degrees of nodes belonging to the projection set, while Full models constraints the degrees of nodes in both sets. Hard or microcanonical models impose exact constraints, while Soft or canonical models impose them as ensemble averages. BiPCM stands for Bipartite Partial CM and BiCM for Bipartite CM.

	Partial (1 set)	Full (2 sets)
Hard (microcanonical)	Hypergeometric ^{44–46}	Curveball ^{50,51}
Soft (canonical)	BiPCM ⁵⁵	BiCM ^{54,55}

Results and Discussion

We perform the comparison of validation outcomes in the context of co-occurrences for country production networks, following the recent stream of works on economic fitness and complexity^{44,57–60}. In particular, our empirical bipartite system is defined by two set of nodes, scientific fields (set L) and world countries (set Γ), and by links that connect countries with the scientific fields they have a comparative advantage on. The L-projection of this bipartite network is a monopartite network of scientific fields, whose generic link C_{ij} is the co-occurrence of fields i and j worldwide. Figure 1 summarizes how the validation procedure is applied to this network. For a description of raw data and pre-processing, see the Methods section.

We start by recalling the key assumption underlying economic complexity studies on co-occurrences: if two scientific fields feature significant co-occurrences (in terms of an appropriate null model) then we can assume that there is an overlap between the capabilities required to achieve proficient level (*i.e.*, competitive advantage) in both fields⁶⁰. The need for statistical validation arises in this context since both countries and scientific fields are heterogeneous (if nothing, by their size): two scientific fields may happen to co-occur in many countries just because they are popular worldwide. Therefore, a reasonable baseline choice of null model is the (bipartite) CM, for which degrees (*i.e.*, the ubiquity of fields and possibly the diversification of countries) sum up all the information. The corresponding null hypothesis is thus that fields are independent and there is no capability structure behind the network: co-occurrences between scientific fields happen at random, some more likely than others just because of their ubiquities or countries’ diversification. Therefore, any specific observed link i, j for which we can reject such null hypothesis is interpreted as the signal of some real interdependence between the specific capabilities required to make proficient scientific research in fields i and j .

Different models, different validated networks

In order to better understand how the validation procedure works, we begin by comparing in Figure 2 the empirical value of the co-occurrences C_{ij} with the respective null model distribution $\pi(\cdot|i, j)$ for some representative pairs i, j of scientific fields. We

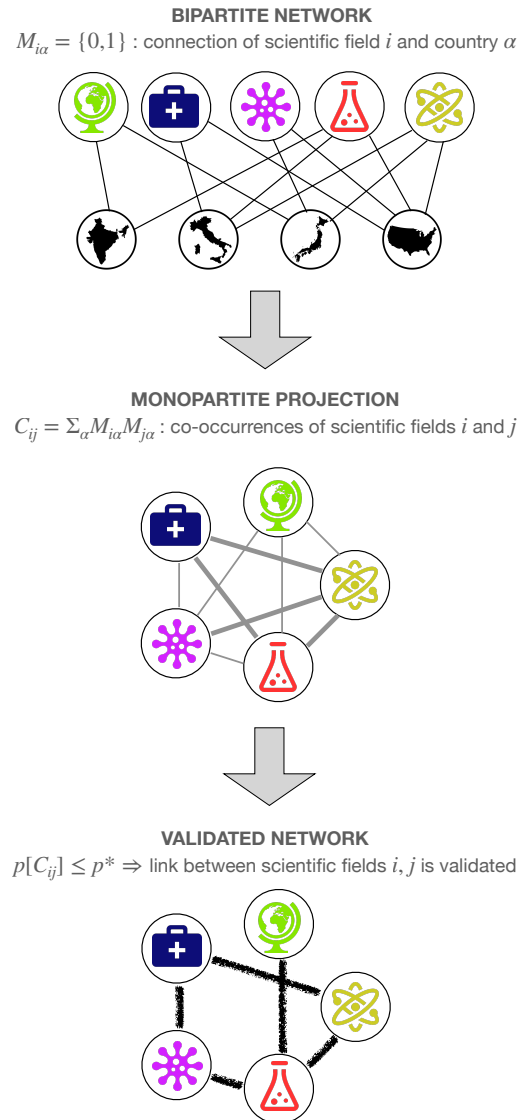


Figure 1. Schematic illustration of the validation procedure for the bipartite network of scientific fields and world countries. We start from the bipartite network \mathbf{M} of scientific fields (in this example: *Earth Sciences*, *Medicine*, *Biology*, *Chemistry* and *Physics*¹¹¹) and world countries (here: India, Italy, Japan, United States¹¹²). In this network, links connect countries with the scientific fields they have a comparative advantage on. From this bipartite structure we create a monopartite projected network \mathbf{C} of scientific fields, whose weighted links represent the co-occurrences of field pairs in the various countries. Finally we assess the statistical significance of each observed co-occurrence against its null model expectation: we place a link on the validated network only when the p -value is smaller than the significance threshold p^* . Note that this procedure is general and applies to any bipartite network.

recall that C_{ij} is validated if it satisfies the condition $p[C_{ij}] \leq p^*$, that is, if the area under the distribution starting from the empirical value is smaller than the threshold p^* . The three example we report are the co-occurrences of: (a) *Mathematical Physics - Geometry and Topology*, which are likely validated, in accordance with our expectations that the two fields are related by requiring common skills and capabilities; (b) *Mathematical Physics - Aquatic Science*, which are likely not validated, again as we can expect that the two fields are unrelated; and (c) *Finance - Applied Psychology*, whose relatedness is plausible but the outcome of the validation procedure is uncertain, as it strongly depends not only on the choice of the threshold p^* but also on the choice of the null model. This is a first evidence that different models may lead to different validated networks.

These plots also highlight some important symmetries between the various null model distributions (see also Figure 3). On one hand, the peaks coincide for the two partial models (Hypergeometric and BiPCM), since they have the same average

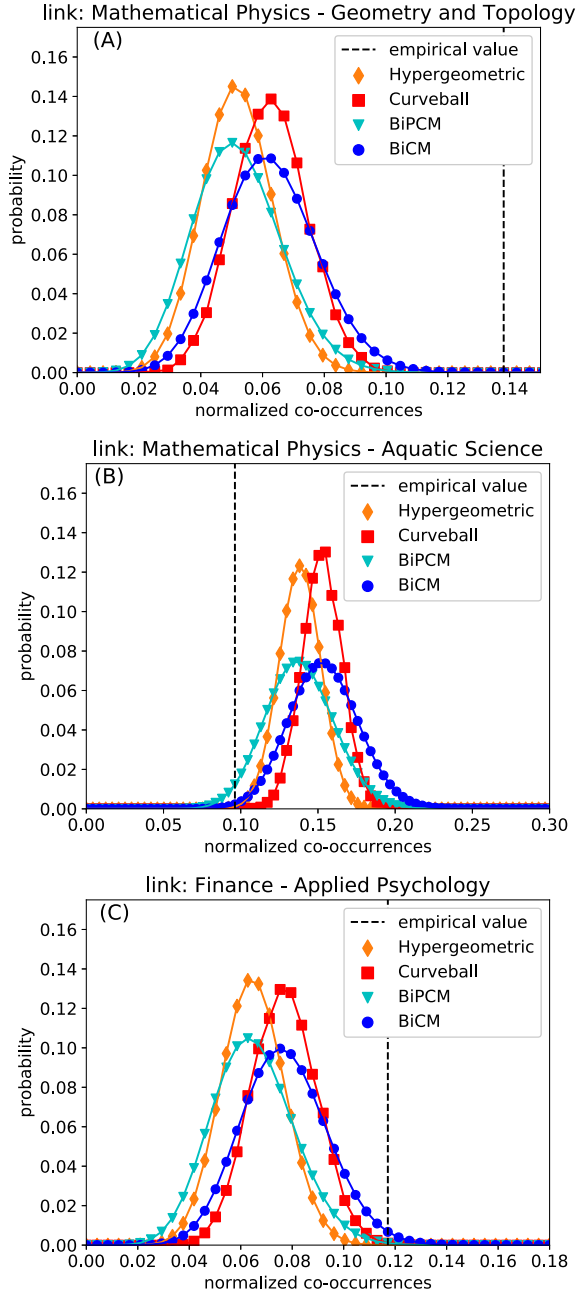


Figure 2. Comparison of empirical co-occurrences and their null model distributions for representative scientific field pairs. (a) *Mathematical Physics - Geometry and Topology*, (b) *Mathematical Physics - Aquatic Science*, (c) *Finance - Applied Psychology*. For each pair (i, j) of scientific fields we report the empirical value of the (normalized) co-occurrences $C_{ij}/|\Gamma|$ and the respective null model distributions $\pi(\cdot|i, j)$. The p-value is given by the area under the distribution starting from the empirical value, hence the outcome of the validation procedure strongly depends both on the significance threshold p^* and the choice of the null model.

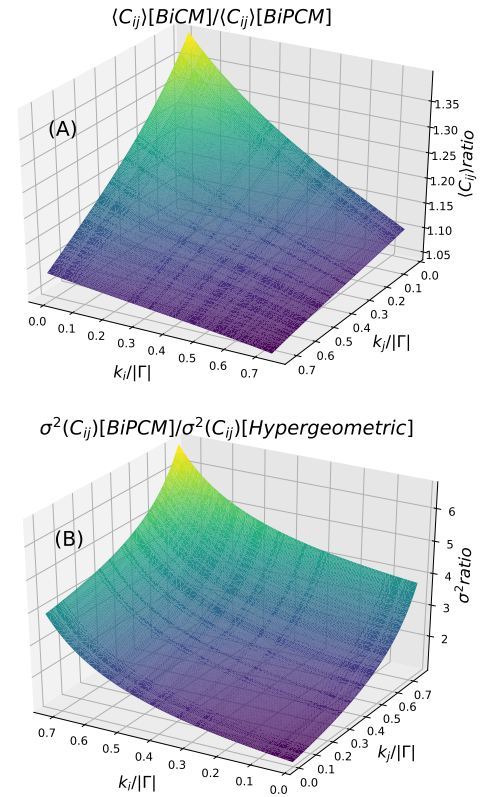


Figure 3. Comparison of null model features. (a) Ratio of mean co-occurrences $\langle C_{ij} \rangle$ for BiCM and BiPCM, and (b) ratio of variances $\sigma^2(C_{ij})$ for BiPCM and Hypergeometric, as a function of the normalized degrees $k_i/|\Gamma|$ and $k_j/|\Gamma|$ of the corresponding nodes. Both quantities are strongly dependent on the specific model formulations, especially for high values of the degrees.

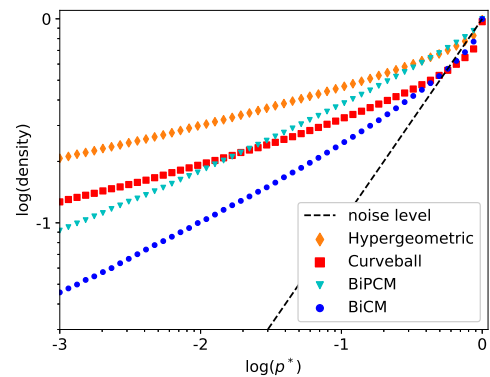


Figure 4. Density ρ of links validated by the various null models as a function of the significance threshold p^* . The dashed bisector denotes the noise level, namely the probability to statistically validate a link generated by the null model. The four null models leads to different results even for the same p^* value.

value $\langle C_{ij} \rangle = k_i k_j / |\Gamma|$ (see eqs. (6) and (14)), but the same also happens for the two full models (Curveball and BiCM). This means that the average value of the co-occurrences in the null model depends on the set(s) on which degree constraints are imposed. Besides, such average is higher for full models as they capture the heterogeneity of both sets. This can be readily seen by taking the sparse limit of the BiCM, for which eq. (9) becomes $p_{i\alpha} \simeq e^{-\theta_i + \alpha} = k_i \kappa_\alpha / E$. Inserting this expression into eq. (11) we get $\langle C_{ij} \rangle \simeq k_i k_j \sum_\alpha \kappa_\alpha^2 / E^2$, which is greater than $\langle C_{ij} \rangle = k_i k_j / |\Gamma|$ of the BiPCM (and equal only when set Γ has no heterogeneity, that is, $\kappa_\alpha = E / |\Gamma| \forall \alpha$). On the other hand, the width of the distribution looks similar for microcanonical models (Hypergeometric and Curveball) and for canonical models (BiPCM and BiCM), implying that the standard deviation of the co-occurrences depends on the types of constraints. As expected, the choice of hard constraints leads to a narrower distribution while the choice of soft constraints leads to a broader distribution. This is easily seen by taking the ratio of variances for the BiPCM (Binomial) and Hypergeometric model, which after some simple algebra can be written as $(|\Gamma|^2 - k_i k_j) / [(|\Gamma| - k_i)(|\Gamma| - k_j)] > 1$. Further insights on model comparison are provided in Supplementary Note 3. Overall, these differences between the null model distributions are likely to produce strong disagreement between the validated networks.

After focusing on individual co-occurrences, we ask in general how many co-occurrences are validated by each null model. We thus measure the link density $\rho(p^*)$ of the validated network, defined as the fraction of i, j pairs such that $p[C_{ij}] \leq p^*$, as a function of the significance threshold p^* . Results for the various null models, reported in Figure 4, show patterns that are consistent with the above observations. The width of the null model distributions sets the slope of the curves, so that BiCM is the model that validates the least by having longer tails and higher mean, whereas Hypergeometric validates the most by having shorter tails and lower mean. Note also that the Hypergeometric ρ does not tend to 0 for $p^* \rightarrow 0$: this is due to the distribution not vanishing within its finite support, whereas the effective support of the canonical models distribution is much larger due to the softness of the imposed constraints. Upstream of these considerations, we observe a very large difference in density between the various null models, even of one order of magnitude for the same p^* values. We can thus conclude that the different null models unavoidably lead to different filtered network structures, even when correcting for multiple hypothesis testing (see Supplementary Note 4).

Null models reconciliation

We now discuss a general methodology to reconcile the four validation schemes. The idea is to find a coherence area in the space of parameters where the filtered networks show a relatively good agreement. We start by assessing the structural similarity of the validated networks using three popular metrics of graph distance⁶¹. The first one is the simple Jaccard coefficient, which measures the number of links in common between two graphs. Jaccard is a known node-correspondence method, *i.e.*, it requires that the two graphs have the same node set and the pairwise correspondence between nodes is known (our validated networks satisfy this requirement). We further consider: *DeltaCon*⁶², another known node-correspondence method based on the comparison of l -length paths connecting each node pair (we use the approximated version of the algorithm, which restricts the computation to randomly chosen pairs); and *Portrait Divergence*⁶³, an unknown node-correspondence method that compares the distribution of the shortest-path lengths between graphs. Any of these methods takes as input the adjacency matrices \mathbf{V} and \mathbf{V}' of two networks, each validated by a different null model, and returns a measure of their similarity $s_{\mathbf{V}\mathbf{V}'} \in [0, 1]$, where $s_{\mathbf{V}\mathbf{V}'} = 0$ means the two networks are maximally different while $s_{\mathbf{V}\mathbf{V}'} = 1$ that they are identical. We can then obtain a mean similarity score by averaging over the six possible choices of null model pairs. A key issue in this comparison is how to choose the validated networks to match. The simplest choice is to compare networks obtained with the same significance threshold p^* , and study the average similarity as a function of p^* (Figure 5, magenta triangles). We see that the average similarity is rather low, especially for Portrait Divergence. In order to recover some compatibility between the results of the different models, we can repeat the operations described above by taking validated networks with the same value of the link density ρ (that is, we adjust p^* for each network in order to obtain the match of ρ values). The resulting curves (green stars in Figure 5) show that the average similarity of networks at equal ρ is always much higher than for networks at equal p^* .

We further study whether the validated networks are similar in terms of mesoscale or community structure. We choose this benchmark because statistical validation on networks is precisely meant to highlight the emergence of multiple-nodes patterns like motifs and communities. Broadly speaking, a community structure is defined by (typically non-overlapping) sets of nodes, characterized by having many more internal links — connecting nodes belonging to the same community — than external links — which connect nodes of different communities²⁶. In order to find the best partition of the network nodes, a number of community detection algorithms have been proposed in the literature (we remand to²⁶ for a recent review of the field). Here we use the popular Louvain method⁶⁴, which is based on maximizing the quality function known as *Modularity*⁶⁵, defined as the observed fraction of links internal to communities with respect to a random benchmark. As there is no community detection method that performs best in all situations^{66,67}, in the Supplementary Note 5 we repeat the same analysis using community inference with Bayesian stochastic blockmodeling⁶⁸ (finding qualitatively similar results).

Figure 6 shows the results of the Louvain algorithm applied on the networks validated by the various null models. Given

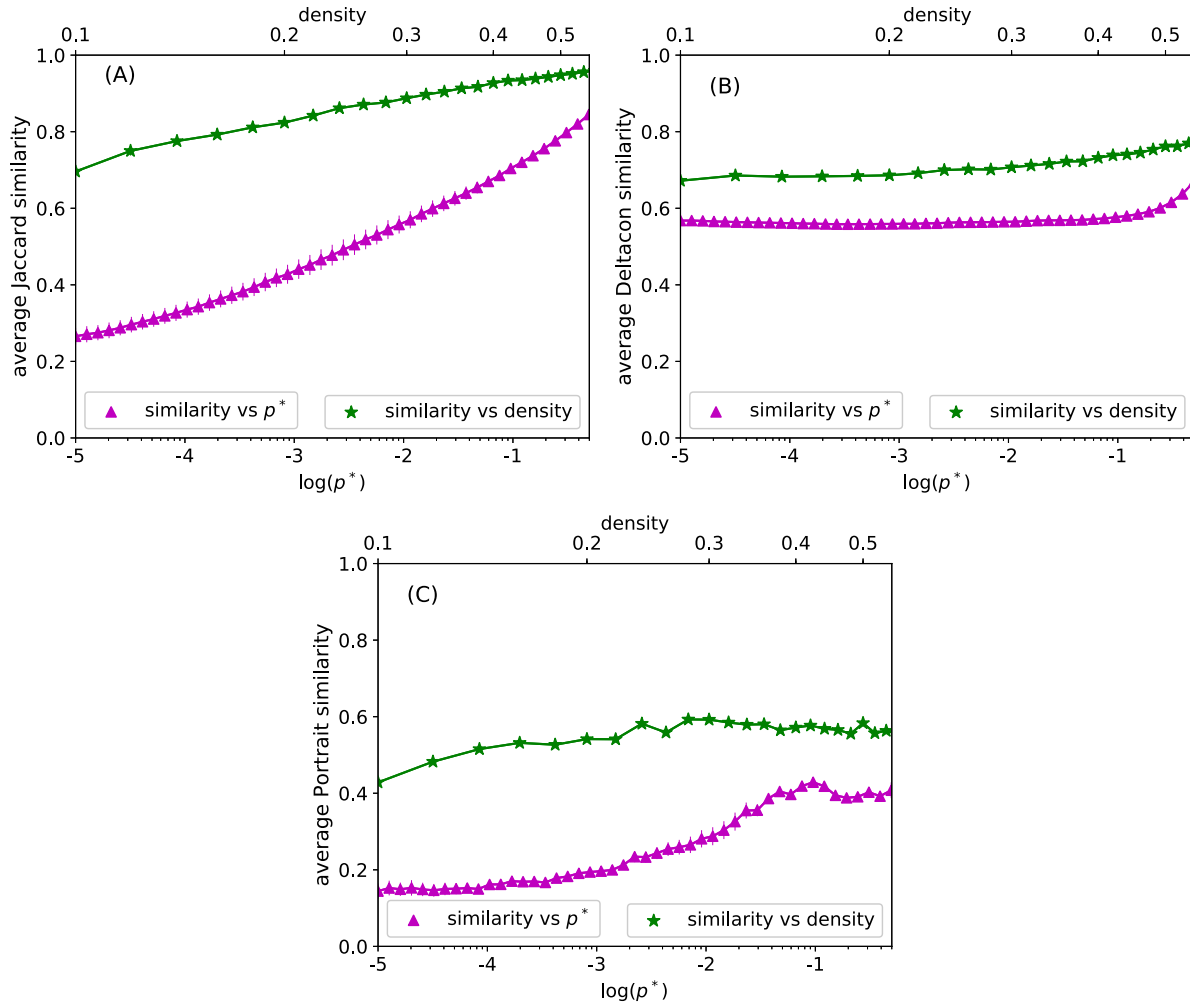


Figure 5. Average structural similarity of the networks validated by the various null models. Error bars (not visible) represent standard deviations over choices of null model pairs. Similarity values measured through (a) Jaccard; (b): DeltaCon; (c): Portrait are plotted for filtered networks obtained with the same significance threshold p^* (magenta triangles) or of equal density (green stars). The latter option reveals a higher concordance among the null models. Note how similarity has a baseline dependence on the network density: a change of a link has more impact in lower density graphs.

the previous analysis on structural similarity, we use ρ rather than p^* as independent variable with the aim of achieving a better compatibility between the results of the different models. In each plot, full circles represent the modularity of the best network partition, which increases as the network becomes more sparse, whereas the solid line marks the number of communities, which also increases for decreasing density due to the appearance of more disconnected components. A nontrivial feature that is common to all plots is the presence of a plateau at 4 communities for $0.1 \lesssim \rho \lesssim 0.3$. Additionally, modularity tends to stabilize at the lower extreme of this plateau. In order to understand whether a community structure common to all null models emerges in this region, we show in Figure 7 the modularity as a function of the number of detected communities. Using this visualization we get rid of the trivial dependence of modularity and number of communities on ρ , and we observe a clear collapse of the curves corresponding to the four models. Additionally we see that modularity, after a fast increase, practically stops to grow after 4 communities are reached (the growth resumes only for a much larger number of communities). This observation points in the direction of a shared community structure. However we still do not know if the partitions identified in each null model setup are actually similar to each other.

To quantify the similarity between different partitions we use the *Adjusted Mutual Information* (AMI)⁶⁹. We choose this metric as it discounts the agreement between partitions solely due to chance, and it is also relatively stable with respect to the

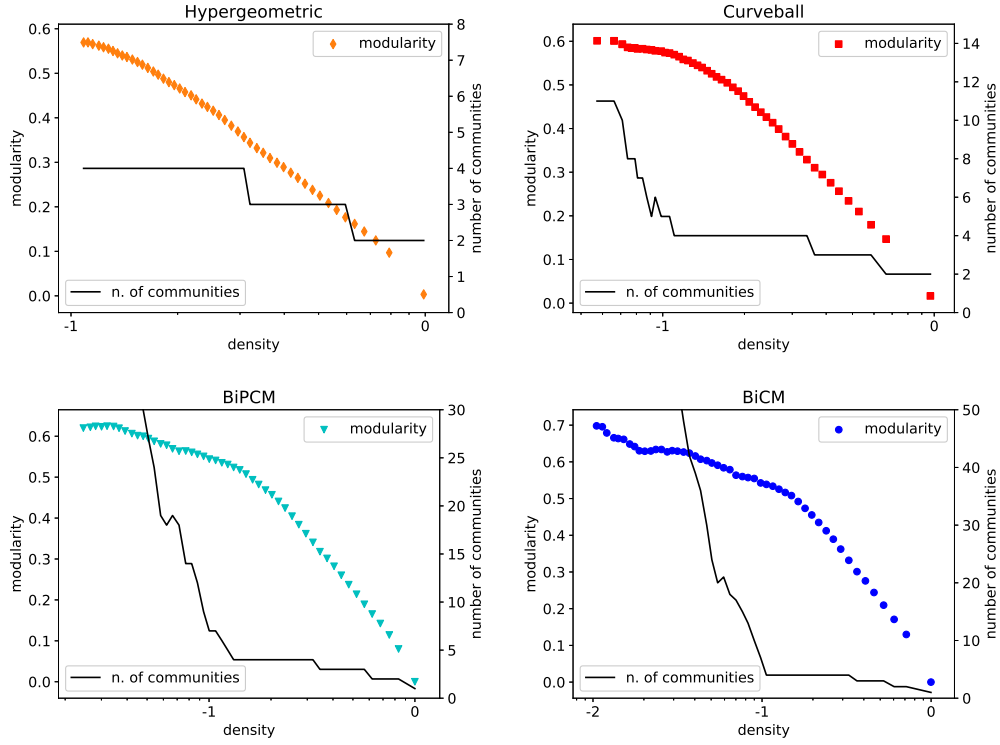


Figure 6. Modularity and number of communities for the best partition obtained by the Louvain method on the validated network, as a function of the density ρ of validated links. Each point corresponds to the partition of highest modularity obtained in 100 runs of the algorithm with random initialization (hence it has no associated error). While modularity monotonically decreases with the density, we observe that the number of communities has a plateau at 4 for $0.1 \lesssim \rho \lesssim 0.3$, suggesting the presence of a region where an agreement between the four approaches is recovered.

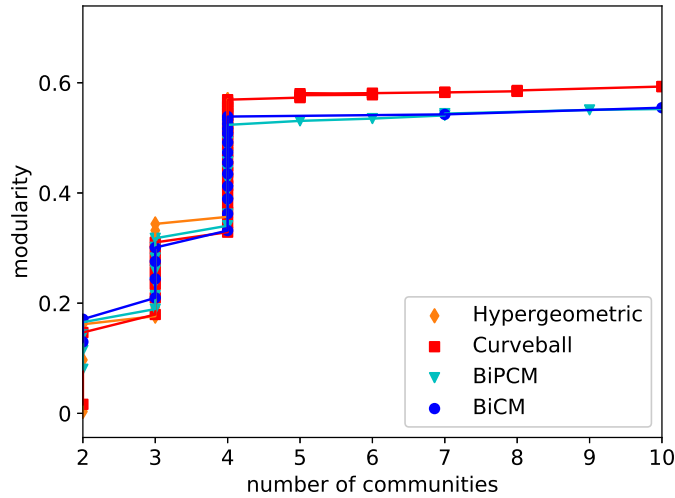


Figure 7. Modularity vs number of communities for the best partition obtained on the validated networks. Note how the curves of the various models collapse onto each other. Besides, the growth of modularity suddenly stops at 4 communities, suggesting the presence of a robust partition shared between all null models.

presence of disconnected components⁷⁰. Given two network partitions U_1 and U_2 , their AMI is defined as

$$\text{AMI}(U_1, U_2) = \frac{\text{MI}(U_1, U_2) - \mathcal{E}\{\text{MI}(U_1, U_2)\}}{\max\{\text{H}(U_1), \text{H}(U_2)\} - \mathcal{E}\{\text{MI}(U_1, U_2)\}} \quad (4)$$

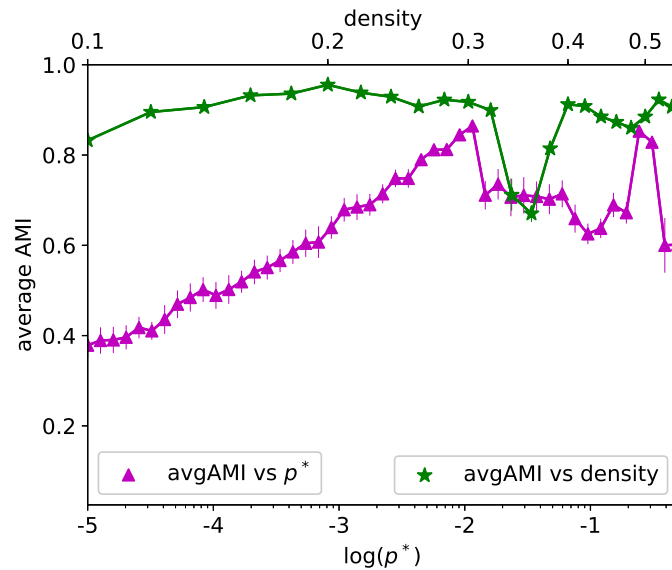


Figure 8. Average Adjusted Mutual Information (AMI) between the best partitions of the network validated by the various null models. Error bars represent standard deviations over choices of null model pairs. Values are plotted for filtered networks obtained with the same significance threshold p^* (magenta triangles) or of equal density (green stars). The latter option reveals a higher concordance among the null models.

where $MI(U_1, U_2)$ is the mutual information between U_1 and U_2 ⁷¹ while $H(U_1)$ and $H(U_2)$ is the Shannon entropy associated with U_1 and U_2 , respectively. The adjustment consists in discounting the expected value $\mathcal{E}\{MI(U_1, U_2)\}$ of the mutual information between two random partitions with the same number of nodes per community as U_1 and U_2 . This correction is needed since the baseline value of mutual information between two random partitions is not constant but grows with the number of communities⁶⁹. AMI varies between 0 (if the observed partitions are consistent with a random labelling) and 1 (if the two partitions coincide).

We can thus take a pair of networks each validated using a given null model, extract the respective best partitions (of highest modularity) and compute their AMI. In analogy to what we did for structural similarity metrics, we compare networks that are either validated with the same significance threshold p^* , or have the same density (that is, we adjust p^* for each network in order to obtain the match of ρ values). We perform this operation for the six possible choices of null model pairs to obtain an average AMI value. Results as a function of p^* or ρ (Figure 8, magenta triangles or green stars, respectively) confirm that the density ρ , and not p^* , is the right knob to turn for finding an agreement among the models. Indeed the average AMI computed for networks at equal ρ is almost always higher than AMI for networks at equal p^* — the only exception being the region around $\rho \simeq 0.3$ where the number of detected communities switches from 4 to 3 but not simultaneously for all models. We can also identify a maximum AMI for $\rho \sim 0.2$, corresponding to the shared community structure illustrated in Figure 9. Hence the four filtering techniques, which in general produce very different statistically validated networks, can be reconciled by choosing model-specific p^* such that the resulting densities of the validated networks are approximately equal and the AMI is maximum. This strategy is rather general and, in principle, can be applied to any bipartite to monopartite projection in order to produce a “meta-validated” filtered network that maximizes the agreement between the different filtering techniques. Even more importantly, it can resolve the arbitrariness in the choice of the significance threshold p^* .

To further support the general applicability of our framework, we show in the Supplementary Note 6 the same analysis performed to several other bipartite networks belonging to totally different contexts. In all cases we find that both the structural similarity and the AMI of the network partition are consistently higher when computed at equal ρ than when obtained at equal p^* . Additionally, when modularity is high enough, a robust community structure shared among the null models emerges.

Conclusions

The increasing availability of complex data we are experiencing nowadays calls for techniques to extract meaningful information from large-scale networks of interactions. The statistical validation of networks is based on comparing empirically observed patterns with their distributional expectation under a null network model. This allows performing a statistical test of whether empirical data is explained by the model or represent additional information. A statistically validated network is built by retaining only the structurally relevant interactions for which the null hypothesis is rejected. This can be of crucial importance

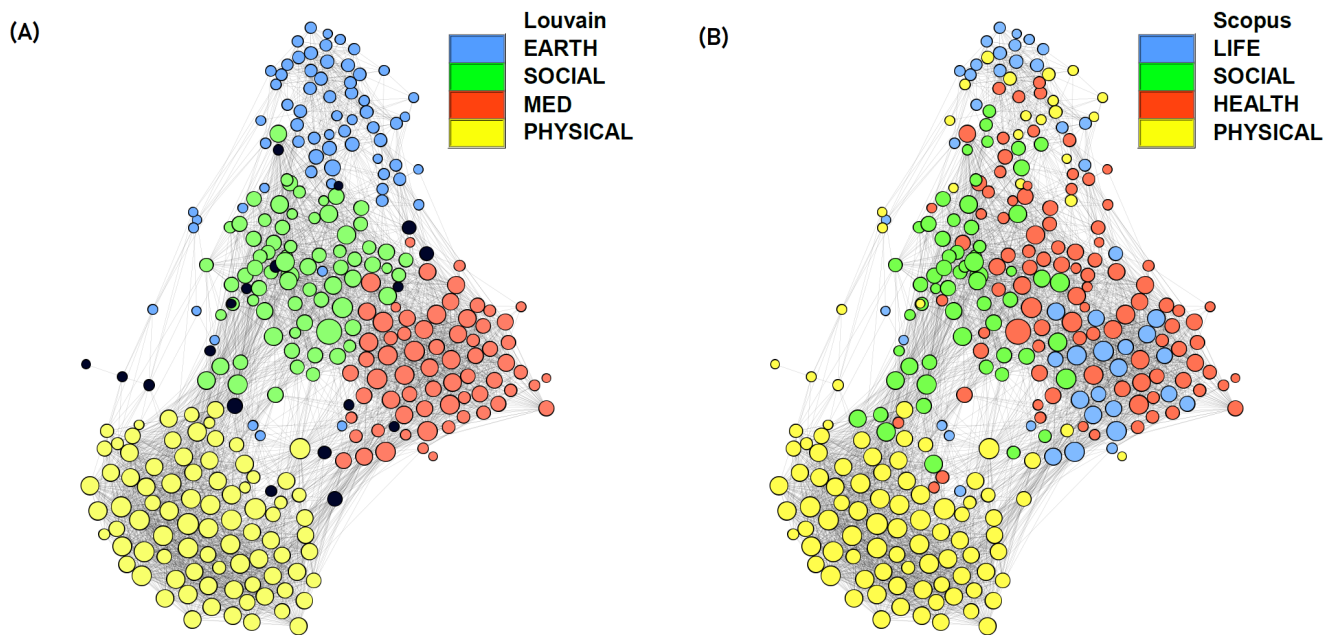


Figure 9. Community structure of the network of co-occurrence between scientific fields, validated by the Hypergeometric null model. The link density is $\rho = 0.2$, corresponding to the maximum adjusted mutual information (AMI) value of Figure 8. (a) Each color identifies a community (hand-labeled by us as in the legend) shared among the four validated networks, whereas the few black nodes denote the mismatches. The network is represented using a force atlas layout. (b) As a comparison, we report the same network with scientific fields labeled according to their ASJC (All Science Journal Classification) subject area assigned by Scopus' in-house experts. Visually, the community structure defined by such classification is not much coherent with the network partition induced by our meta-validation approach based on significant co-occurrences, which we recall links two scientific fields when they require common capabilities.

to obtain simpler and clearer descriptions of complex systems³⁴.

For instance, statistical validation of bipartite network projections has been used to detect important patterns in financial markets, such as preferential or avoided relationships^{72,73}, clusters of investors characterized by the same investment profile⁷⁴⁻⁷⁶, and overlapping portfolios bearing the highest riskiness for fire sales liquidation⁵⁴. In the context of economic and innovation systems, validated network projections have been used to detect modules of countries with similar industrial profile and the hierarchical structure of products and services^{55,77}, traces of specialisations emerging from the baseline diversification strategy of countries⁷⁸, and predictive innovation patterns involving the interplay of scientific, technological and economic activities⁶⁰. In the context of mobile communications, validated networks were shown to be more resilient than ordinary networks to errors⁷⁹.

Naturally, any null model hinges on a definition of what type of information represents a signal as opposed to noise. As a result, the validated networks obtained through different filtering techniques carry different meanings and highlight different properties. Even different constructions of the same null model may yield different outcomes. This latter issue has been recently shown in the context of nestedness in ecological systems¹⁷: whether the degree sequence is responsible for the nestedness of a bipartite network^{80,81} depends on the choice of the CM-based null model ensemble (microcanonical or canonical)⁸². The non-equivalence between the microcanonical and canonical ensembles is due to the extensive number of constraints (one for each network node) and holds also in the thermodynamic limit⁸³⁻⁸⁵.

In this work we have reviewed (using a unified notation) the CM-based null model formulations for bipartite network projections, and performed a systematic comparison in terms of null model characteristics and validation outcomes within the same contexts. We showed that the different model formulations lead to different validation results, both at the level of individual links and of macroscale network properties (see also this recent preprint⁸⁶). However we do provide a recipe to reconcile the validation outcomes, by comparing networks obtained with model-specific significance thresholds such that the density of validated links becomes comparable. Additionally this comparison may allow to identify the region of density values where the agreement between models is maximum. On one hand this solves the arbitrariness in the choice of the significance threshold. On the other hand, it offers a meta-validation approach to identify the filtered configurations with the highest signal-to-noise ratio.

We have included in our comparative study CM-based null models defined on one or both sets of the bipartite network, as well as those defined directly on the monopartite projection, considering in all cases both hard and soft constraints. Note that, in principle, “softer” constraints could be imposed by fixing the functional form of the degree distribution rather than the degree sequence, as in the *hypersoft* CM^{87–89}. This approach may be more adequate in the case of dynamic networks, in which degree sequences are never fixed but their distributions are often stable. Developing a hypersoft CM for bipartite networks and projections, and adding it to our meta-validation framework represents a promising research direction. Additional challenges for future research are represented by the development of suitable models for weighted bipartite networks and their projections^{90,91}, as well as the extension of validation methods beyond pairwise interactions^{92,93}.

As long-term goal we plan to investigate whether the proposed meta-validation approach allows not only to capture the most relevant structural properties of the network projection, but also to help in predicting its evolution – namely, which links will appear in the future. This could be important in various contexts, from link prediction for recommender systems based on collaborative filtering^{12,94} to assessing prices trend and systemic risk in financial networks of portfolios and assets^{54,95} and forecasting development patterns in economic and innovation systems^{60,96,97}.

Methods

Null Models of Bipartite Network Projections

Here we provide the mathematical definitions of the null models used in our analysis.

Microcanonical Partial Model: Hypergeometric. For the projection of a bipartite network on set L, an analytic null hypothesis can be formulated by assuming random connections between nodes of the two sets L and Γ that preserve the degree heterogeneity of set L^{44,46}. Under this hypothesis, the probability that nodes i and j have x co-occurrences is given by the hypergeometric distribution

$$\pi(x|i, j) = \binom{k_i}{x} \binom{|\Gamma| - k_i}{k_j - x} / \binom{|\Gamma|}{k_j} \quad (5)$$

and the mean value of the co-occurrences is

$$\langle C_{ij} \rangle = k_i k_j / |\Gamma|. \quad (6)$$

This probability is exact only when nodes of set Γ have the same degree. A tentative extension to deal with the degree heterogeneity of set Γ consists in splitting the original bipartite network into subnetworks each consisting of set Γ nodes with the same degree and of all set L nodes linked to them, so that the null hypothesis can be properly cast for each subnetwork⁴⁶. However, when set Γ is highly heterogeneous these subnetworks are many in number and very sparse, causing severe resolution issues (see the discussion in⁵⁴).

Microcanonical Full model: Curveball. Building a null bipartite network model where only configurations with a given degree sequence for both sets of nodes are allowed has not been tackled analytically up to now (exact results exist only in the thermodynamic limit concerning the count of bipartite graphs with given degree sequences⁹⁸). This model is hard to deal with because, differently from the canonical case (see below), link probabilities are not pairwise independent. Therefore the model must be defined through an ensemble of bipartite network configurations that are generated numerically by swapping links iteratively so to preserve degrees exactly. The *Curveball* algorithm^{50–52} works as follows: Starting from the empirical bipartite network \mathbf{M} , these steps are repeated n times:

1. Select at random a pair of nodes i, j in set L;
2. Check that the neighborhoods of the nodes are not perfectly overlapping (otherwise start again);
3. Take the set of uncommon neighbors $\delta(i, j) = \{\alpha \in \Gamma | M_{i\alpha} \oplus M_{j\alpha} = 1\}$ and remove them from the neighborhood of both;
4. Assign $k_i - \sum_{\alpha} M_{i\alpha} M_{j\alpha}$ new neighbors to node i , chosen at random from $\delta(i, j)$, and the rest of the nodes in $\delta(i, j)$ to node j .

The result is a randomized bipartite network configuration $\tilde{\mathbf{M}}$ (here and in what follows we use the tilde symbol to denote matrix configurations of the null model). This procedure is repeated iteratively to generate an ensemble $\{\tilde{\mathbf{M}}_q\}_{q=1}^Q$ of Q independent randomizations of the bipartite network. The null model ensemble $\{\tilde{\mathbf{C}}_r\}_{r=1}^R$ of projected networks is then obtained by projecting pairs of different instances of bipartite randomizations (that is, a generic configuration is obtained as $\tilde{\mathbf{C}}_r = \tilde{\mathbf{M}}_q \tilde{\mathbf{M}}_{q'}^T$ with $q \neq q'$).

The null model distributions $\pi(\cdot|i, j) \forall i, j$ are then computed numerically by sampling from such an ensemble. Here we use $n = 5 \min\{|\mathbf{L}|, |\Gamma|\}$ and $Q = R = 10000$. Note that for a numerically-generated ensemble of R network configurations, the minimum p-value that can be used for statistical testing is $1/R$.

Canonical Full model: BiCM. Generally speaking, canonical models of networks^{43,99–101} (also known as *exponential random graphs*^{102–104}) define an ensemble Ω of networks using a constrained entropy maximization procedure, which leads to assuming the utmost ignorance about the unconstrained degrees of freedom of the system^{34,105}. The Bipartite Configuration Model (BiCM)⁵³ applies to bipartite networks by constraining the ensemble average of the degree sequence for both node sets. The ensemble probability distribution that maximizes the Shannon entropy under these constraints is

$$P(\tilde{\mathbf{M}}|\{\theta_i\}, \{t_\alpha\}) = e^{-H(\tilde{\mathbf{M}}, \{\theta_i\}, \{t_\alpha\})} / Z(\{\theta_i\}, \{t_\alpha\}) \quad (7)$$

where $\{\theta_i\}$ and $\{t_\alpha\}$ are the sets of Lagrange multipliers associated to the constraints $\{k_i\}$ and $\{\kappa_\alpha\}$ respectively, $Z(\{\theta_i\}, \{t_\alpha\}) = \sum_{\tilde{\mathbf{M}} \in \Omega} e^{-H(\tilde{\mathbf{M}}, \{\theta_i\}, \{t_\alpha\})}$ is the partition function and the Hamiltonian $H(\tilde{\mathbf{M}}, \{\theta_i\}, \{t_\alpha\}) = \sum_{i \in \mathbf{L}} \theta_i k_i(\tilde{\mathbf{M}}) + \sum_{\alpha \in \Gamma} t_\alpha \kappa_\alpha(\tilde{\mathbf{M}})$ sums up the imposed constraints. Note that $P(\tilde{\mathbf{M}}|\{\theta_i\}, \{t_\alpha\})$ depends on $\tilde{\mathbf{M}}$ only through $k_i(\tilde{\mathbf{M}})$ and $\kappa_\alpha(\tilde{\mathbf{M}})$: network configurations with the same value of the constraints are equiprobable, which implies that the canonical ensemble is maximally non-committal (or the least biased) with respect to the properties that are not enforced on the system. Since degrees are linear constraints the partition function can be computed analytically, so the ensemble probability factorizes as

$$P(\tilde{\mathbf{M}}|\{\theta_i\}, \{t_\alpha\}) = \prod_{i, \alpha} p_{i\alpha}^{\tilde{M}_{i\alpha}} (1 - p_{i\alpha})^{1 - \tilde{M}_{i\alpha}} \quad (8)$$

where $p_{i\alpha}$ is the existence probability of the link connecting nodes i and α :

$$p_{i\alpha} = (e^{\theta_i + t_\alpha} + 1)^{-1}. \quad (9)$$

The numerical values of the link probabilities (*i.e.*, of the Lagrange multipliers) are determined by maximising the likelihood of the empirical bipartite network \mathbf{M} in the ensemble, which implies solving the constraints equations

$$\begin{cases} k_i = \sum_{\alpha \in \Gamma} p_{i\alpha} & i \in \mathbf{L} \\ \kappa_\alpha = \sum_{i \in \mathbf{L}} p_{i\alpha} & \alpha \in \Gamma \end{cases} \quad (10)$$

Once link probabilities have been found, the expected co-occurrences between any two nodes $i \neq j$ are

$$\langle C_{ij} \rangle = \sum_{\alpha \in \Gamma} p_{i\alpha} p_{j\alpha}, \quad (11)$$

and the probability distribution $\pi(\cdot|i, j)$ of this quantity is the distribution of the sum of Γ independent Bernoulli trials, each with success probability $p_{i\alpha} p_{j\alpha}$. This is a Poisson-Binomial distribution, which can be computed numerically⁵⁴ or analytically⁵⁵ as

$$\pi(x|i, j) = \sum_{\gamma_x} \left[\prod_{\alpha \in \gamma_x} p_{i\alpha} p_{j\alpha} \prod_{\beta \notin \gamma_x} (1 - p_{i\beta} p_{j\beta}) \right] \quad (12)$$

where γ_x denotes all possible x -tuples of nodes in set Γ .

Canonical Partial model: BiPCM. The “partial” version of the BiCM, named BiPCM in ref.⁵⁵, is defined as the canonical model that constrains only the degree sequence of set \mathbf{L} . As such, it is a special case of the BiCM described above where all Lagrange multipliers $\{t_\alpha\}$ associated with degrees of set Γ are “switched off” (*i.e.*, set equal to zero). The Hamiltonian is thus $H(\tilde{\mathbf{M}}, \{\theta_i\}) = \sum_{i \in \mathbf{L}} \theta_i k_i(\tilde{\mathbf{M}})$ and the link probability of generic link (i, α) becomes $p_{i\alpha} = (e^{\theta_i} + 1)^{-1}$. Using the constraint equations $k_i = \sum_{\alpha \in \Gamma} p_{i\alpha} \forall i \in \mathbf{L}$ we get the explicit expression

$$p_{i\alpha} = k_i / |\Gamma| \quad \forall i \in \mathbf{L}. \quad (13)$$

Therefore the expected value of the co-occurrence between any two nodes i and j is

$$\langle C_{ij} \rangle = k_i k_j / |\Gamma| \quad (14)$$

and its distribution has a simple Binomial form

$$\pi(x|i, j) = \binom{|\Gamma|}{x} \left(\frac{k_i k_j}{|\Gamma|^2} \right)^x \left(1 - \frac{k_i k_j}{|\Gamma|^2} \right)^{|\Gamma| - x} \quad (15)$$

Data, RCA filter and Projection

To build the bipartite network of countries and scientific fields, we use data on scientific productivity and impact of countries collected from the SCIMAGO platform (based on Scopus). The database contains the corpus of scientific publications in journals, book series, conference proceedings, and books in the various scientific fields, covering the time interval from 1996 to 2018. Data are then aggregated at the level of countries and scientific fields (in total there are $|\mathcal{L}| = 307$ scientific fields and $|\mathcal{I}| = 239$ countries), so that $W_{i\alpha}$ is the total number of scientific documents produced by country α in scientific field i during the time span of the data.

In order to determine whether a given country α shows a comparative advantage in field i , both with respect to other countries as well as to other fields, the *revealed comparative advantage* (RCA)¹⁰⁶ filter comes at hand. While originally developed in the economic context, this metric has also found use in studies of scientific production^{60,107,108}. RCA is an intensive indicator computed as the ratio between the weight of field i in the scientific basket of country α and the weight of field i in the total world science. As a comparative advantage is revealed if $RCA > 1$, we binarize the raw matrices to obtain new matrices

$$M_{i\alpha} = \begin{cases} 1 & \text{if } \frac{W_{i\alpha}}{\sum_j W_{j\alpha}} / \frac{\sum_\beta W_{i\beta}}{\sum_{j\beta} W_{j\beta}} \geq 1, \\ 0 & \text{otherwise.} \end{cases} \quad (16)$$

Note that the RCA filter is properly normalized by making quantities related to different countries and fields comparable¹⁰⁹.

Once the binary bipartite matrix is defined, we build the projected network of co-occurrences between scientific fields, whose generic connection between fields i and j is $C_{ij} = \sum_\alpha M_{i\alpha} M_{j\alpha}$. Note that for the sake of having a clearer picture and more analytical insights on the various null models, we do not employ here more refined formulations of co-occurrences that use additional normalization by degrees^{57,59,60}.

Acknowledgments. We thank Benedetta Castagna and Aurelio Patelli for useful discussion. We acknowledge the CREF project "Complessità in Economia" and the ISC-CNR project "CompLang".

Author contributions. GC and AZ designed the research. AC and LD performed research. AC realised the figures. GC wrote the manuscript. GC, AC and AZ reviewed the manuscript.

Data availability. The dataset about scientific productivity of countries analysed during the current study can be obtained from SCImago, (n.d.). SJR - SCImago Journal & Country Rank [Portal], which can be retrieved at <https://www.scimagojr.com/countryrank.php>. The other datasets analyzed in the Supplementary Note 6 are available at the web addresses indicated in the same document.

Code availability. The code to run the Curveball algorithm can be retrieved from⁵¹, while the code to run BiCM is available at <https://github.com/tsakim/bicm> (Hypergeometric and BiPCM have analytic formulas). Codes for computing network distance metrics can be retrieved from⁶¹ while the code for computing Modularity and AMI are available respectively at <https://github.com/taynaud/python-louvain> and <https://scikit-learn.org/stable/modules/clustering.html#mutual-info-score>¹¹⁰. Network visualizations have been generated using Gephi <https://gephi.org>.

References

1. Song, C., Havlin, S. & Makse, H. A. Self-similarity of complex networks. *Nature* **433**, 392–395, DOI: [10.1038/nature03248](https://doi.org/10.1038/nature03248) (2005).
2. Boccaletti, S., Latora, V., Moreno, Y., Chavez, M. & Hwang, D.-U. Complex networks: Structure and dynamics. *Phys. Reports* **424**, 175–308, DOI: [10.1016/j.physrep.2005.10.009](https://doi.org/10.1016/j.physrep.2005.10.009) (2006).
3. Dorogovtsev, S. N., Goltsev, A. V. & Mendes, J. F. F. Critical phenomena in complex networks. *Rev. Mod. Phys.* **80**, 1275–1335, DOI: [10.1103/RevModPhys.80.1275](https://doi.org/10.1103/RevModPhys.80.1275) (2008).

4. Pastor-Satorras, R., Castellano, C., Van Mieghem, P. & Vespignani, A. Epidemic processes in complex networks. *Rev. Mod. Phys.* **87**, 925–979, DOI: [10.1103/RevModPhys.87.925](https://doi.org/10.1103/RevModPhys.87.925) (2015).
5. Benson, A. R., Gleich, D. F. & Leskovec, J. Higher-order organization of complex networks. *Science* **353**, 163–166, DOI: [10.1126/science.aad9029](https://doi.org/10.1126/science.aad9029) (2016).
6. Barabási, A.-L. The network takeover. *Nat. Phys.* **8**, 14–16, DOI: [10.1038/nphys2188](https://doi.org/10.1038/nphys2188) (2012).
7. Newman, M. *Networks* (Oxford university press, 2018).
8. Caldarelli, G. A perspective on complexity and networks science. *J. Physics: Complex.* **1**, 021001, DOI: [10.1088/2632-072x/ab9a24](https://doi.org/10.1088/2632-072x/ab9a24) (2020).
9. Holme, P., Liljeros, F., Edling, C. R. & Kim, B. J. Network bipartivity. *Phys. Rev. E* **68**, 056107, DOI: [10.1103/PhysRevE.68.056107](https://doi.org/10.1103/PhysRevE.68.056107) (2003).
10. Faust, K. Centrality in affiliation networks. *Soc. Networks* **19**, 157–191, DOI: [10.1016/S0378-8733\(96\)00300-0](https://doi.org/10.1016/S0378-8733(96)00300-0) (1997).
11. Newman, M. E. J. Coauthorship networks and patterns of scientific collaboration. *Proc. Natl. Acad. Sci.* **101**, 5200–5205, DOI: [10.1073/pnas.0307545100](https://doi.org/10.1073/pnas.0307545100) (2004).
12. Zhou, T., Ren, J., Medo, M. & Zhang, Y.-C. Bipartite network projection and personal recommendation. *Phys. Rev. E* **76**, 046115, DOI: [10.1103/PhysRevE.76.046115](https://doi.org/10.1103/PhysRevE.76.046115) (2007).
13. Bardoscia, M. *et al.* The physics of financial networks. *Nat. Rev. Phys.* **3**, 490–507, DOI: [10.1038/s42254-021-00322-5](https://doi.org/10.1038/s42254-021-00322-5) (2021).
14. Hidalgo, C. A. & Hausmann, R. The building blocks of economic complexity. *Proc. Natl. Acad. Sci.* **106**, 10570–10575, DOI: [10.1073/pnas.0900943106](https://doi.org/10.1073/pnas.0900943106) (2009).
15. Tacchella, A., Cristelli, M., Caldarelli, G., Gabrielli, A. & Pietronero, L. A new metrics for countries' fitness and products' complexity. *Sci. Reports* **2**, 723, DOI: [10.1038/srep00723](https://doi.org/10.1038/srep00723) (2012).
16. Ings, T. C. *et al.* Review: Ecological networks – beyond food webs. *J. Animal Ecol.* **78**, 253–269, DOI: [10.1111/j.1365-2656.2008.01460.x](https://doi.org/10.1111/j.1365-2656.2008.01460.x) (2009).
17. Mariani, M. S., Ren, Z.-M., Bascompte, J. & Tessone, C. J. Nestedness in complex networks: Observation, emergence, and implications. *Phys. Reports* **813**, 1–90, DOI: [10.1016/j.physrep.2019.04.001](https://doi.org/10.1016/j.physrep.2019.04.001) (2019).
18. Goh, K.-I. *et al.* The human disease network. *Proc. Natl. Acad. Sci.* **104**, 8685–8690, DOI: [10.1073/pnas.0701361104](https://doi.org/10.1073/pnas.0701361104) (2007).
19. Pavlopoulos, G. A. *et al.* Bipartite graphs in systems biology and medicine: a survey of methods and applications. *GigaScience* **7**, DOI: [10.1093/gigascience/giy014](https://doi.org/10.1093/gigascience/giy014) (2018).
20. Vasques Filho, D. & O'Neale, D. R. J. Degree distributions of bipartite networks and their projections. *Phys. Rev. E* **98**, 022307, DOI: [10.1103/PhysRevE.98.022307](https://doi.org/10.1103/PhysRevE.98.022307) (2018).
21. Kruskal, J. B. On the shortest spanning subtree of a graph and the traveling salesman problem. *Proc. Am. Math. society* **7**, 48–50, DOI: [10.2307/2033241](https://doi.org/10.2307/2033241) (1956).
22. Tumminello, M., Aste, T., Di Matteo, T. & Mantegna, R. N. A tool for filtering information in complex systems. *Proc. Natl. Acad. Sci.* **102**, 10421–10426, DOI: [10.1073/pnas.0500298102](https://doi.org/10.1073/pnas.0500298102) (2005).
23. Maslov, S. & Sneppen, K. Specificity and stability in topology of protein networks. *Science* **296**, 910–913, DOI: [10.1126/science.1065103](https://doi.org/10.1126/science.1065103) (2002).
24. Milo, R. *et al.* Network motifs: Simple building blocks of complex networks. *Science* **298**, 824–827, DOI: [10.1126/science.298.5594.824](https://doi.org/10.1126/science.298.5594.824) (2002).
25. Serrano, M. A., Boguñá, M. & Vespignani, A. Extracting the multiscale backbone of complex weighted networks. *PNAS* **106**, 6483–6488, DOI: [10.1073/pnas.0808904106](https://doi.org/10.1073/pnas.0808904106) (2009).
26. Fortunato, S. & Hric, D. Community detection in networks: A user guide. *Phys. Reports* **659**, 1–44, DOI: [10.1016/j.physrep.2016.09.002](https://doi.org/10.1016/j.physrep.2016.09.002) (2016).
27. MacMahon, M. & Garlaschelli, D. Community detection for correlation matrices. *Phys. Rev. X* **5**, 021006, DOI: [10.1103/PhysRevX.5.021006](https://doi.org/10.1103/PhysRevX.5.021006) (2015).
28. Bongiorno, C., London, A., Miccichè, S. & Mantegna, R. N. Core of communities in bipartite networks. *Phys. Rev. E* **96**, 022321, DOI: [10.1103/PhysRevE.96.022321](https://doi.org/10.1103/PhysRevE.96.022321) (2017).

29. Vázquez, A. *et al.* The topological relationship between the large-scale attributes and local interaction patterns of complex networks. *Proc. Natl. Acad. Sci.* **101**, 17940–17945, DOI: [10.1073/pnas.0406024101](https://doi.org/10.1073/pnas.0406024101) (2004).
30. Foster, D. V., Foster, J. G., Grassberger, P. & Paczuski, M. Clustering drives assortativity and community structure in ensembles of networks. *Phys. Rev. E* **84**, 066117, DOI: [10.1103/PhysRevE.84.066117](https://doi.org/10.1103/PhysRevE.84.066117) (2011).
31. Colomer-de Simón, P., Serrano, M. Á., Beiró, M. G., Alvarez-Hamelin, J. I. & Boguñá, M. Deciphering the global organization of clustering in real complex networks. *Sci. Reports* **3**, 2517, DOI: [10.1038/srep02517](https://doi.org/10.1038/srep02517) (2013).
32. Orsini, C. *et al.* Quantifying randomness in real networks. *Nat. Commun.* **6**, 8627, DOI: [10.1038/ncomms9627](https://doi.org/10.1038/ncomms9627) (2015).
33. Marcaccioli, R. & Livan, G. A pólya urn approach to information filtering in complex networks. *Nat. Commun.* **10**, 745, DOI: [10.1038/s41467-019-08667-3](https://doi.org/10.1038/s41467-019-08667-3) (2019).
34. Cimini, G. *et al.* The statistical physics of real-world networks. *Nat. Rev. Phys.* **1**, 58–71, DOI: [10.1038/s42254-018-0002-6](https://doi.org/10.1038/s42254-018-0002-6) (2019).
35. Colizza, V., Flammini, A., Serrano, M. A. & Vespignani, A. Detecting rich-club ordering in complex networks. *Nat. Phys.* **2**, 110, DOI: [10.1038/nphys209](https://doi.org/10.1038/nphys209) (2006).
36. Nunes Amaral, L. A. & Guimera, R. Lies, damned lies and statistics. *Nat. Phys.* **2**, 75–76, DOI: [10.1038/nphys228](https://doi.org/10.1038/nphys228) (2006).
37. Erdős, P. & Rényi, A. On random graphs. *Publ. Math. Debrecen* **6**, 290–297 (1959).
38. Latapy, M., Magnien, C. & Vecchio, N. D. Basic notions for the analysis of large two-mode networks. *Soc. Networks* **30**, 31–48, DOI: [10.1016/j.socnet.2007.04.006](https://doi.org/10.1016/j.socnet.2007.04.006) (2008).
39. Neal, Z. Identifying statistically significant edges in one-mode projections. *Soc. Netw. Analysis Min.* **3**, 915–924, DOI: [10.1007/s13278-013-0107-y](https://doi.org/10.1007/s13278-013-0107-y) (2013).
40. Serafino, M. *et al.* True scale-free networks hidden by finite size effects. *Proc. Natl. Acad. Sci.* **118**, DOI: [10.1073/pnas.2013825118](https://doi.org/10.1073/pnas.2013825118) (2021).
41. Chung, F. & Lu, L. Connected components in random graphs with given expected degree sequences. *Annals Comb.* **6**, 125–145, DOI: [10.1007/PL00012580](https://doi.org/10.1007/PL00012580) (2002).
42. Newman, M. E. J., Strogatz, S. H. & Watts, D. J. Random graphs with arbitrary degree distributions and their applications. *Phys. Rev. E* **64**, 026118, DOI: [10.1103/PhysRevE.64.026118](https://doi.org/10.1103/PhysRevE.64.026118) (2001).
43. Squartini, T. & Garlaschelli, D. Analytical maximum-likelihood method to detect patterns in real networks. *New J. Phys.* **13**, 083001, DOI: [10.1088/1367-2630/13/8/083001](https://doi.org/10.1088/1367-2630/13/8/083001) (2011).
44. Teece, D. J., Rumelt, R., Dosi, G. & Winter, S. Understanding corporate coherence: Theory and evidence. *J. Econ. Behav. Organ.* **23**, 1–30, DOI: [10.1016/0167-2681\(94\)90094-9](https://doi.org/10.1016/0167-2681(94)90094-9) (1994).
45. Goldberg, D. S. & Roth, F. P. Assessing experimentally derived interactions in a small world. *Proc. Natl. Acad. Sci.* **100**, 4372–4376, DOI: [10.1073/pnas.0735871100](https://doi.org/10.1073/pnas.0735871100) (2003).
46. Tumminello, M., Miccichè, S., Lillo, F., Piilo, J. & Mantegna, R. N. Statistically validated networks in bipartite complex systems. *PLoS ONE* **6**, e17994, DOI: [10.1371/journal.pone.0017994](https://doi.org/10.1371/journal.pone.0017994) (2011).
47. Neal, Z. The backbone of bipartite projections: Inferring relationships from co-authorship, co-sponsorship, co-attendance and other co-behaviors. *Soc. Networks* **39**, 84–97, DOI: [10.1016/j.socnet.2014.06.001](https://doi.org/10.1016/j.socnet.2014.06.001) (2014).
48. Zweig, K. A. & Kaufmann, M. A systematic approach to the one-mode projection of bipartite graphs. *Soc. Netw. Analysis Min.* **1**, 187–218, DOI: [10.1007/s13278-011-0021-0](https://doi.org/10.1007/s13278-011-0021-0) (2011).
49. Gionis, A., Mannila, H., Mielikäinen, T. & Tsaparas, P. Assessing data mining results via swap randomization. *ACM Trans. Knowl. Discov. Data* **1**, DOI: [10.1145/1297332.1297338](https://doi.org/10.1145/1297332.1297338) (2007).
50. Verhelst, N. D. An efficient mcmc algorithm to sample binary matrices with fixed marginals. *Psychometrika* **73**, 705, DOI: [10.1007/s11336-008-9062-3](https://doi.org/10.1007/s11336-008-9062-3) (2008).
51. Strona, G., Nappo, D., Boccacci, F., Fattorini, S. & San-Miguel-Ayanz, J. A fast and unbiased procedure to randomize ecological binary matrices with fixed row and column totals. *Nat. communications* **5**, 4114 (2014).
52. Carstens, C. J. Proof of uniform sampling of binary matrices with fixed row sums and column sums for the fast curveball algorithm. *Phys. Rev. E* **91**, 042812, DOI: [10.1103/PhysRevE.91.042812](https://doi.org/10.1103/PhysRevE.91.042812) (2015).
53. Saracco, F., Di Clemente, R., Gabrielli, A. & Squartini, T. Randomizing bipartite networks: The case of the world trade web. *Sci. Reports* **5**, 10595, DOI: [10.1038/srep10595](https://doi.org/10.1038/srep10595) (2015).

54. Gualdi, S., Cimini, G., Primicerio, K., Di Clemente, R. & Challet, D. Statistically validated network of portfolio overlaps and systemic risk. *Sci. Reports* **6**, 39467, DOI: [10.1038/srep39467](https://doi.org/10.1038/srep39467) (2016).
55. Saracco, F. *et al.* Inferring monopartite projections of bipartite networks: An entropy-based approach. *New J. Phys.* **19**, 053022, DOI: [10.1088/1367-2630/aa6b38](https://doi.org/10.1088/1367-2630/aa6b38) (2017).
56. Mastrandrea, R., Squartini, T., Fagiolo, G. & Garlaschelli, D. Enhanced reconstruction of weighted networks from strengths and degrees. *New J. Phys.* **16**, 043022, DOI: [10.1088/1367-2630/16/4/043022](https://doi.org/10.1088/1367-2630/16/4/043022) (2014).
57. Hidalgo, C. A., Klinger, B., Barabási, A.-L. & Hausmann, R. The product space conditions the development of nations. *Science* **317**, 482–487, DOI: [10.1126/science.1144581](https://doi.org/10.1126/science.1144581) (2007).
58. Klimek, P., Hausmann, R. & Thurner, S. Empirical confirmation of creative destruction from world trade data. *PLoS ONE* **7**, e38924, DOI: [10.1371/journal.pone.0038924](https://doi.org/10.1371/journal.pone.0038924) (2012).
59. Zaccaria, A., Cristelli, M., Tacchella, A. & Pietronero, L. How the taxonomy of products drives the economic development of countries. *PLoS ONE* **9**, e113770, DOI: [10.1371/journal.pone.0113770](https://doi.org/10.1371/journal.pone.0113770) (2014).
60. Pugliese, E. *et al.* Unfolding the innovation system for the development of countries: co-evolution of science, technology and production. *Sci. Reports* **9**, 16440, DOI: [10.1038/s41598-019-52767-5](https://doi.org/10.1038/s41598-019-52767-5) (2019).
61. Tantardini, M., Ieva, F., Tajoli, L. & Piccardi, C. Comparing methods for comparing networks. *Sci. Reports* **9**, 17557, DOI: [10.1038/s41598-019-53708-y](https://doi.org/10.1038/s41598-019-53708-y) (2019).
62. Koutra, D., Shah, N., Vogelstein, J. T., Gallagher, B. & Faloutsos, C. Deltacon: Principled massive-graph similarity function with attribution. *ACM Trans. Knowl. Discov. Data* **10**, DOI: [10.1145/2824443](https://doi.org/10.1145/2824443) (2016).
63. Bagrow, J. P. & Bollt, E. M. An information-theoretic, all-scales approach to comparing networks. *Appl. Netw. Sci.* **4**, 45, DOI: [10.1007/s41109-019-0156-x](https://doi.org/10.1007/s41109-019-0156-x) (2019).
64. Blondel, V. D., Guillaume, J.-L., Lambiotte, R. & Lefebvre, E. Fast unfolding of communities in large networks. *J. statistical mechanics: theory experiment* **2008**, P10008, DOI: [10.1088/1742-5468/2008/10/P10008](https://doi.org/10.1088/1742-5468/2008/10/P10008) (2008).
65. Newman, M. E. Modularity and community structure in networks. *Proc. Natl. Acad. Sci.* **103**, 8577–8582, DOI: [10.1073/pnas.0601602103](https://doi.org/10.1073/pnas.0601602103) (2006).
66. Peel, L., Larremore, D. B. & Clauset, A. The ground truth about metadata and community detection in networks. *Sci. Adv.* **3**, e1602548, DOI: [10.1126/sciadv.1602548](https://doi.org/10.1126/sciadv.1602548) (2017).
67. Ghasemian, A., Hosseinmardi, H. & Clauset, A. Evaluating overfit and underfit in models of network community structure. *IEEE Trans. on Knowl. Data Eng.* **32**, 1722–1735, DOI: [10.1109/TKDE.2019.2911585](https://doi.org/10.1109/TKDE.2019.2911585) (2020).
68. Peixoto, T. P. Efficient monte carlo and greedy heuristic for the inference of stochastic block models. *Phys. Rev. E* **89**, 012804, DOI: [10.1103/PhysRevE.89.012804](https://doi.org/10.1103/PhysRevE.89.012804) (2014).
69. Vinh, N. X., Epps, J. & Bailey, J. Information theoretic measures for clusterings comparison: Variants, properties, normalization and correction for chance. *The J. Mach. Learn. Res.* **11**, 2837–2854, DOI: [10.5555/1756006.1953024](https://doi.org/10.5555/1756006.1953024) (2010).
70. Romano, S., Bailey, J., Nguyen, V. & Verspoor, K. Standardized mutual information for clustering comparisons: One step further in adjustment for chance. In *Proceedings of the 31st International Conference on International Conference on Machine Learning - Volume 32*, II–1143–II–1151, DOI: [10.5555/3044805.3045020](https://doi.org/10.5555/3044805.3045020) (JMLR.org, 2014).
71. Strehl, A. & Ghosh, J. Cluster ensembles — a knowledge reuse framework for combining multiple partitions. *J. Mach. Learn. Res.* **3**, 583–617, DOI: [10.1162/153244303321897735](https://doi.org/10.1162/153244303321897735) (2003).
72. Hatzopoulos, V., Iori, G., Mantegna, R. N., Miccichè, S. & Tumminello, M. Quantifying preferential trading in the e-mid interbank market. *Quant. Finance* **15**, 693–710, DOI: [10.1080/14697688.2014.969889](https://doi.org/10.1080/14697688.2014.969889) (2015).
73. Musciotto, F., Piilo, J. & Mantegna, R. N. High-frequency trading and networked markets. *Proc. Natl. Acad. Sci.* **118**, DOI: [10.1073/pnas.2015573118](https://doi.org/10.1073/pnas.2015573118) (2021).
74. Tumminello, M., Lillo, F., Piilo, J. & Mantegna, R. N. Identification of clusters of investors from their real trading activity in a financial market. *New J. Phys.* **14**, 013041, DOI: [10.1088/1367-2630/14/1/013041](https://doi.org/10.1088/1367-2630/14/1/013041) (2012).
75. Musciotto, F., Marotta, L., Miccichè, S., Piilo, J. & Mantegna, R. N. Patterns of trading profiles at the nordic stock exchange. a correlation-based approach. *Chaos, Solitons & Fractals* **88**, 267–278, DOI: <https://doi.org/10.1016/j.chaos.2016.02.027> (2016).
76. Musciotto, F., Marotta, L., Piilo, J. & Mantegna, R. N. Long-term ecology of investors in a financial market. *Palgrave Commun.* **4**, 92, DOI: [10.1057/s41599-018-0145-1](https://doi.org/10.1057/s41599-018-0145-1) (2018).

77. Zaccaria, A., Mishra, S., Cader, M. Z. & Pietronero, L. Integrating services in the economic fitness approach. *World Bank Policy Res. Work. Pap.* (2018).
78. Straka, M. J., Caldarelli, G. & Saracco, F. Grand canonical validation of the bipartite international trade network. *Phys. Rev. E* **96**, 022306, DOI: [10.1103/PhysRevE.96.022306](https://doi.org/10.1103/PhysRevE.96.022306) (2017).
79. Li, M.-X. *et al.* Statistically validated mobile communication networks: the evolution of motifs in european and chinese data. *New J. Phys.* **16**, 083038, DOI: [10.1088/1367-2630/16/8/083038](https://doi.org/10.1088/1367-2630/16/8/083038) (2014).
80. Jonhson, S., Domínguez-García, V. & Muñoz, M. A. Factors determining nestedness in complex networks. *PLoS ONE* **8**(9), e74025, DOI: [10.1371/journal.pone.0074025](https://doi.org/10.1371/journal.pone.0074025) (2013).
81. Payrató-Borràs, C., Hernández, L. & Moreno, Y. Breaking the spell of nestedness: The entropic origin of nestedness in mutualistic systems. *Phys. Rev. X* **9**, 031024, DOI: [10.1103/PhysRevX.9.031024](https://doi.org/10.1103/PhysRevX.9.031024) (2019).
82. Bruno, M., Saracco, F., Garlaschelli, D., Tessone, C. J. & Caldarelli, G. The ambiguity of nestedness under soft and hard constraints. *Sci. Reports* **10**, 19903, DOI: [10.1038/s41598-020-76300-1](https://doi.org/10.1038/s41598-020-76300-1) (2020).
83. Barré, J. & Gonçalves, B. Ensemble inequivalence in random graphs. *Phys. A: Stat. Mech. its Appl.* **386**, 212–218, DOI: [10.1016/j.physa.2007.08.015](https://doi.org/10.1016/j.physa.2007.08.015) (2007).
84. Anand, K. & Bianconi, G. Entropy measures for networks: Toward an information theory of complex topologies. *Phys. Rev. E* **80**, 045102, DOI: [10.1103/PhysRevE.80.045102](https://doi.org/10.1103/PhysRevE.80.045102) (2009).
85. Squartini, T., de Mol, J., den Hollander, F. & Garlaschelli, D. Breaking of ensemble equivalence in networks. *Phys. Rev. Lett.* **115**, 268701, DOI: [10.1103/PhysRevLett.115.268701](https://doi.org/10.1103/PhysRevLett.115.268701) (2015).
86. Neal, Z. P., Domagalski, R. & Sagan, B. Comparing models for extracting the backbone of bipartite projections. <https://arxiv.org/abs/2105.13396> (2021).
87. Anand, K., Krioukov, D. & Bianconi, G. Entropy distribution and condensation in random networks with a given degree distribution. *Phys. Rev. E* **89**, 062807, DOI: [10.1103/PhysRevE.89.062807](https://doi.org/10.1103/PhysRevE.89.062807) (2014).
88. van der Hoorn, P., Lippner, G. & Krioukov, D. Sparse maximum-entropy random graphs with a given power-law degree distribution. *J. Stat. Phys.* **173**, 806–844, DOI: [10.1007/s10955-017-1887-7](https://doi.org/10.1007/s10955-017-1887-7) (2018).
89. Voitalov, I., van der Hoorn, P., Kitsak, M., Papadopoulos, F. & Krioukov, D. Weighted hypersoft configuration model. *Phys. Rev. Res.* **2**, 043157, DOI: [10.1103/PhysRevResearch.2.043157](https://doi.org/10.1103/PhysRevResearch.2.043157) (2020).
90. Garlaschelli, D. & Loffredo, M. I. Generalized bose-fermi statistics and structural correlations in weighted networks. *Phys. Rev. Lett.* **102**, 038701, DOI: [10.1103/PhysRevLett.102.038701](https://doi.org/10.1103/PhysRevLett.102.038701) (2009).
91. Gabrielli, A., Mastrandrea, R., Caldarelli, G. & Cimini, G. Grand canonical ensemble of weighted networks. *Phys. Rev. E* **99**, 030301, DOI: [10.1103/PhysRevE.99.030301](https://doi.org/10.1103/PhysRevE.99.030301) (2019).
92. Battiston, F. *et al.* Networks beyond pairwise interactions: Structure and dynamics. *Phys. Reports* **874**, 1–92, DOI: <https://doi.org/10.1016/j.physrep.2020.05.004> (2020).
93. Musciotto, F., Battiston, F. & Mantegna, R. N. Detecting informative higher-order interactions in statistically validated hypergraphs. <https://arxiv.org/abs/2103.16484> (2021).
94. Kobayashi, T., Takaguchi, T. & Barrat, A. The structured backbone of temporal social ties. *Nat. Commun.* **10**, 220, DOI: [10.1038/s41467-018-08160-3](https://doi.org/10.1038/s41467-018-08160-3) (2019).
95. Vodenska, I., Dehmamy, N., Becker, A. P., Buldyrev, S. V. & Havlin, S. Systemic stress test model for shared portfolio networks. *Sci. Reports* **11**, 3358, DOI: [10.1038/s41598-021-82904-y](https://doi.org/10.1038/s41598-021-82904-y) (2021).
96. Tacchella, A., Zaccaria, A., Miccheli, M. & Pietronero, L. Relatedness in the era of machine learning. <https://arxiv.org/abs/2103.06017> (2021).
97. Straccamore, M., Pietronero, L. & Zaccaria, A. Which will be your firm's next technology? comparison between machine learning and network-based algorithms. <https://arxiv.org/abs/2110.02004> (2021).
98. Liebenau, A. & Wormald, N. Asymptotic enumeration of digraphs and bipartite graphs by degree sequence. <https://arxiv.org/abs/2006.15797> (2020).
99. Park, J. & Newman, M. E. J. Statistical mechanics of networks. *Phys. Rev. E* **70**, 066117, DOI: [10.1103/PhysRevE.70.066117](https://doi.org/10.1103/PhysRevE.70.066117) (2004).
100. Bianconi, G. The entropy of randomized network ensembles. *Europhys. Lett.* **81**, 28005, DOI: [10.1209/0295-5075/81/28005](https://doi.org/10.1209/0295-5075/81/28005) (2008).

101. Garlaschelli, D. & Loffredo, M. I. Maximum likelihood: Extracting unbiased information from complex networks. *Phys. Rev. E* **78**, 015101(R), DOI: [10.1103/PhysRevE.78.015101](https://doi.org/10.1103/PhysRevE.78.015101) (2008).
102. Holland, P. W. & Leinhardt, S. An exponential family of probability distributions for directed graphs. *J. Am. Stat. Assoc.* **76**, 33–50, DOI: [10.2307/2287037](https://doi.org/10.2307/2287037) (1981).
103. Strauss, D. On a general class of models for interaction. *SIAM Rev.* **28**, 513–527, DOI: [10.1137/1028156](https://doi.org/10.1137/1028156) (1986).
104. Snijders, T. A. B., Pattison, P. E., Robins, G. L. & Handcock, M. S. New specifications for exponential random graph models. *Sociol. Methodol.* **36**, 99–153, DOI: [10.1111/j.1467-9531.2006.00176.x](https://doi.org/10.1111/j.1467-9531.2006.00176.x) (2006).
105. Jaynes, E. T. Information theory and statistical mechanics. *Phys. Rev.* **106**, 620–630, DOI: [10.1103/PhysRev.106.620](https://doi.org/10.1103/PhysRev.106.620) (1957).
106. Balassa, B. Trade liberalisation and “revealed” comparative advantage. *The Manch. Sch.* **33**, 99–123, DOI: [10.1111/j.1467-9957.1965.tb00050.x](https://doi.org/10.1111/j.1467-9957.1965.tb00050.x) (1965).
107. Bowen, H. P. On the theoretical interpretation of indices of trade intensity and revealed comparative advantage. *Weltwirtschaftliches Arch.* **119**, 464–472, DOI: [10.1007/BF02706520](https://doi.org/10.1007/BF02706520) (1983).
108. Guevara, M. R., Hartmann, D., Aristarán, M., Mendoza, M. & Hidalgo, C. A. The research space: Using career paths to predict the evolution of the research output of individuals, institutions, and nations. *Scientometrics* **109**, 1695–1709, DOI: [10.1007/s11192-016-2125-9](https://doi.org/10.1007/s11192-016-2125-9) (2016).
109. Radicchi, F., Fortunato, S. & Castellano, C. Universality of citation distributions: Toward an objective measure of scientific impact. *Proc. Natl. Acad. Sci.* **105**, 17268–17272, DOI: [10.1073/pnas.0806977105](https://doi.org/10.1073/pnas.0806977105) (2008).
110. Pedregosa, F. *et al.* Scikit-learn: Machine learning in python. *J. Mach. Learn. Res.* **12**, 2825–2830 (2011).
111. Icons from Iconmonstr <https://iconmonstr.com>
112. Icons from Linseed Studio, NounProject <https://thenounproject.com>

Meta-validation of bipartite network projections: Supplementary Information

Giulio Cimini,^{1,2} Alessandro Carra,³ Luca Didomenicantonio,³ and Andrea Zaccaria^{4,2}

¹Physics Department and INFN, University of Rome Tor Vergata, 00133 Rome (Italy)

²Enrico Fermi Research Center, 00184 Rome (Italy)

³Physics Department, Sapienza University of Rome, 00185 Rome (Italy)

⁴Institute for Complex Systems (CNR) UoS Sapienza, 00185 Rome (Italy)

SUPPLEMENTARY NOTE 1: RIGHT VS LEFT TAIL TEST OF STATISTICAL SIGNIFICANCE

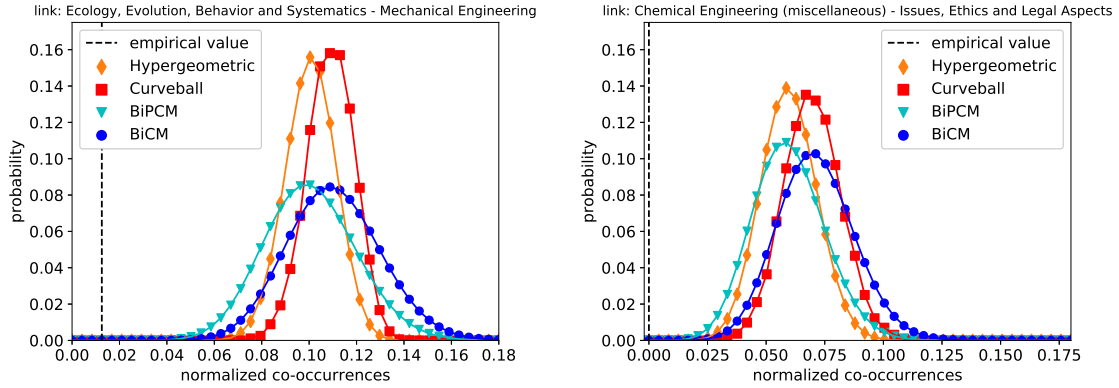
The definition of p-value – same of eq. (3) of the main text

$$p[C_{ij}] = 1 - \sum_{x=0}^{C_{ij}-1} \pi(x|i, j), \quad (\text{S1})$$

is the probability that i and j have no less than C_{ij} co-occurrences in the null model¹. This definition plus the condition of statistical significance $p[C_{ij}] < p^*$ is useful to detect the co-occurrences that are significantly *larger* than their null model expectations. We use such a one-tailed test (the right tail one) because we associate a significantly large value of co-occurrences to a signal of real interdependence between the two nodes involved. Hence, we are not interested in detecting the empirical co-occurrences that are significantly *smaller* than the null model expectations. Nevertheless, it is straightforward to implement the left tail test as well, by defining the p-value as

$$p'[C_{ij}] = \sum_{x=0}^{C_{ij}} \pi(x|i, j), \quad (\text{S3})$$

plus the same condition of statistical significance $p[C_{ij}] < p^*$. The right-hand side of eq. (S3) is now the probability that i and j have no more than C_{ij} co-occurrences in the null model. Differently from the right tail test, however, it



Supplementary Figure 1. Comparison of empirical co-occurrences and their null model distributions for representative scientific field pairs. (left) *Ecology, Evolution, Behavior and Systematics - Mechanical Engineering*, (right) *Chemical Engineering (miscellaneous) - Issues, Ethics and Legal Aspects*. For each pair (i, j) of scientific fields we report the empirical value of the (normalized) co-occurrences $C_{ij}/|\Gamma|$ and the respective null model distributions $\pi(\cdot|i, j)$. For the left tail test, the p-value is given by the area under the distribution up to the empirical value.

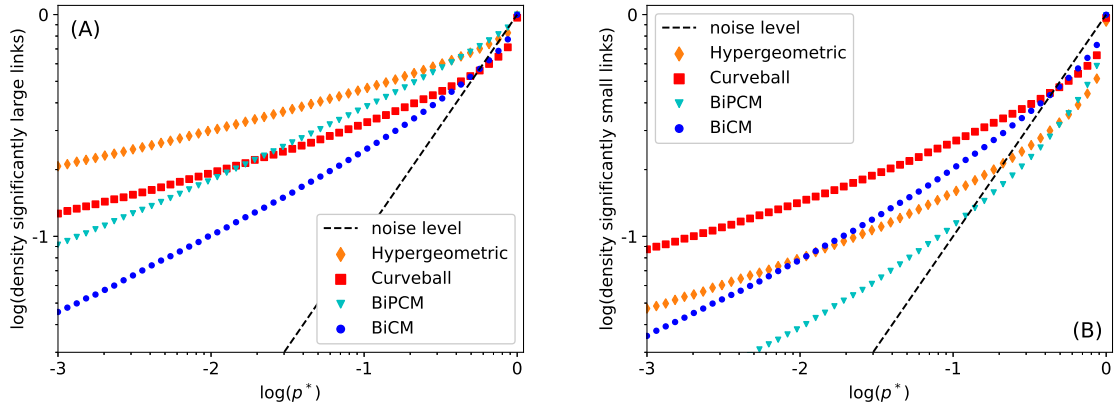
¹ Note that co-occurrences C_{ij} are a discrete variable, therefore the null model distribution $\pi(\cdot|i, j)$ has a discrete support ranging from 0 to $\min[k_i, k_j]$. The p-value definition of eq. (S1) commonly used in the literature is the sum of $\pi(\cdot|i, j)$ starting from the empirical value of C_{ij} included. The other possibility would be to exclude C_{ij} from the sum domain, resulting in

$$p[C_{ij}] = 1 - \sum_{x=0}^{C_{ij}-1} \pi(x|i, j). \quad (\text{S2})$$

The two approaches would coincide if C_{ij} were a continuous variable. In our discrete case, we checked that they lead to almost identical results, after a proper re-scaling of the significance threshold p^* .

is less clear what kind of signal can be associated to the co-occurrences that pass such statistical test. Supplementary Figure 1 shows two example of significantly small co-occurrences between pairs of scientific fields, which appear quite unrelated to each other.

Overall, as shown in Supplementary Figure 2, the number of link validated by the right tail test (panel A – which is the same of Figure 4 in the main text) is typically higher than the number of links validated by the left tail test (panel B), especially for partial models (this happens due to the relative position of the mean between partial and full models). This observation confirms that empirical data on the scientific activity of country is biased towards the right tail and that therefore there is a non-trivial signal of interdependence and common capability requirements between scientific fields.



Supplementary Figure 2. Density ρ of links validated by the various null models as a function of the significance threshold p^* . Panels (A) and (B) report results of the right / left tail test, which validates the links that are significantly larger / smaller than the null model expectations, respectively.

SUPPLEMENTARY NOTE 2: NULL MODELS OF WEIGHTED MONOPARTITE NETWORKS

As discussed in the main text, the task of filtering a bipartite network projection can be in principle accomplished using a null model defined directly on the projection, instead of a null model defined on the original bipartite network. Since the projection of a bipartite network is a (dense) weighted monopartite network, we can use a null model formulation that constrains the strength sequence of the projection, where the strength of generic node i is given by $s_i = \sum_{j(\neq i) \in \mathbb{L}} C_{ij}$. Here we consider two popular model formulations.

Disparity Filter

The *Disparity Filter* [1] relies on the null hypothesis that node i distributes its total strength s_i in a uniform random division among its neighbors. If we denote by d_i the degree of node i in the projected network (*i.e.*, $d_i = \sum_{j(\neq i) \in \mathbb{L}} \Theta[C_{ij}]$ where $\Theta[x] = 1$ if $x > 0$ and $\Theta[x] = 0$ otherwise), the corresponding null model distribution can be expressed as

$$\pi(x|i, j) = \frac{d_i - 1}{s_i} \left(1 - \frac{x}{s_i}\right)^{d_i - 2} \quad (\text{S4})$$

This expression is obtained by considering $d_i - 1$ points distributed with uniform probability in the interval $[0, s_i]$. These points divide this interval into d_i sub-intervals, whose lengths represent the expected values for the d_i weights according to the null hypothesis. Note that differently from the models discussed in the main text, eq. (S4) is not symmetric in i, j and indeed depends only on node i 's properties. Therefore we assign a p-value to the link i, j by averaging the p-values obtained by testing the link from both the perspectives of node i and of node j , that is, $p[C_{ij}] = 1 - \frac{1}{2} \sum_{x=0}^{C_{ij}-1} [\pi(x|i, j) + \pi(x|j, i)]$.

Weighted Configuration Model

The maximum-entropy model that constrains the ensemble average of nodes strength sequence is known as *Weighted Configuration Model* (WCM) [2, 3]. The WCM Hamiltonian is $H(\bar{\mathbf{C}}, \{\eta_i\}) = \sum_{i \in \mathbb{L}} \eta_i s_i(\bar{\mathbf{C}})$ where $\{\eta_i\}$ is the set of Lagrange multipliers associated to the constraints $\{s_i\}$. Also in this case the partition function can be computed analytically and the ensemble probability factorizes into link-specific terms, each of which is simply the probability distribution of the co-occurrences:

$$\pi(x|i, j) = q_{ij}^x (1 - q_{ij}). \quad (\text{S5})$$

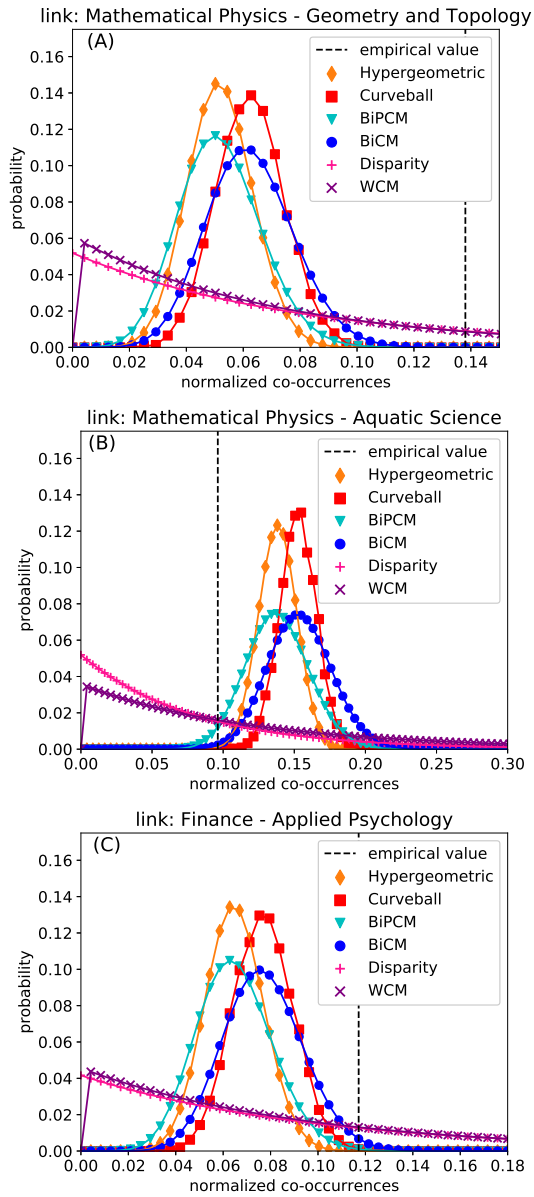
This is a geometric distribution with success probability $q_{ij} = e^{-\eta_i - \eta_j}$ and expected value

$$\langle C_{ij} \rangle = \frac{q_{ij}}{1 - q_{ij}}. \quad (\text{S6})$$

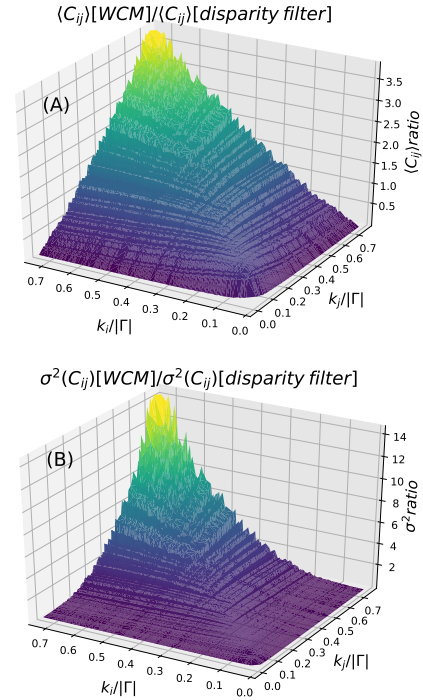
Finally the numerical values of the Lagrange multipliers are determined by maximising the likelihood of the empirical projected network \mathbf{C} in the ensemble, which implies solving the constraints equations $s_i = \sum_{j(\neq i) \in \mathbb{L}} q_{ij} / (1 - q_{ij}) \forall i$.

Comparative analysis of validation outcomes

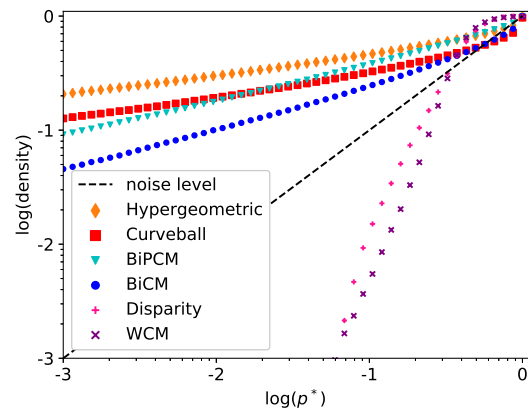
Supplementary Figures 3 and 5 show that the null model distributions for Disparity Filter and WCM feature an extreme positive skewness but also a much longer tail than the bipartite models counterparts. The effect is that they end up validating nothing also for very large significance thresholds p^* . Therefore the information on the bipartite network that originated the projection (which these two models discard) is essential to extract significant information on the projection itself. At last, Supplementary Figure 4 shows that Disparity Filter behaves approximately as a microcanonical model when compared to the canonical WCM.



Supplementary Figure 3. Comparison of empirical co-occurrences and their null model distributions for representative scientific field pairs. (A) *Mathematical Physics - Geometry and Topology*, (B) *Mathematical Physics - Aquatic Science*, (C) *Finance - Applied Psychology*. For each pair (i, j) of scientific field we report the empirical value of the (normalized) co-occurrences $C_{ij}/|\Gamma|$ and the respective null model distributions $\pi(\cdot|i, j)$. This figure is the same of Figure 2 of the main text with the addition of Disparity Filter and WCM.



Supplementary Figure 4. Comparison of null model features. (A) Ratio of average co-occurrences $\langle C_{ij} \rangle$ and (B) ratio of variances $\sigma^2(C_{ij})$ for WCM and Disparity Filter, as a function of the normalized degrees $k_i/|\Gamma|$ and $k_j/|\Gamma|$ of the corresponding nodes.



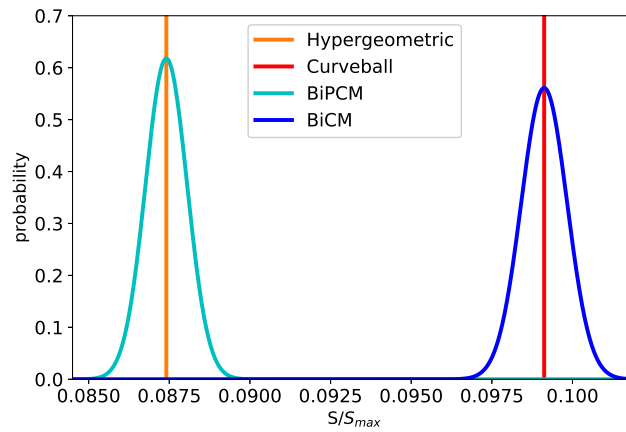
Supplementary Figure 5. Density ρ of links validated by the various null models as a function of the significance threshold p^* . The dashed bisector denotes the noise level, namely the probability to statistically validate a null model event. This figure is the same of Figure 4 of the main text with the addition of Disparity Filter and WCM.

SUPPLEMENTARY NOTE 3: TOTAL CO-OCCURRENCES

Further insights on the features of the various null model formulations can be gained by studying the distribution of the total co-occurrences

$$S = \sum_{\{i,j\} \in L} \langle C_{ij} \rangle. \quad (S7)$$

In agreement with the discussion in the main text, Supplementary Figure 6 shows that these distributions behave very differently for the various null models. The mean of the two partial models (Hypergeometric and BiPCM) coincide, as well as the mean of the two full models (Curveball and BiCM), with the former smaller than the latter. Moreover, microcanonical models (Hypergeometric and Curveball) feature a Dirac delta distribution because of the hardness of imposed constraints. This can be seen by noting that $S \equiv \sum_{\alpha \in \Gamma} \langle k_{\alpha} \rangle^2$, a number which is fixed in both microcanonical ensembles. Canonical models (BiPCM and BiCM) instead feature a similar (finite) standard deviation, very small in comparison with the difference of means so that the respective distribution do not overlap.



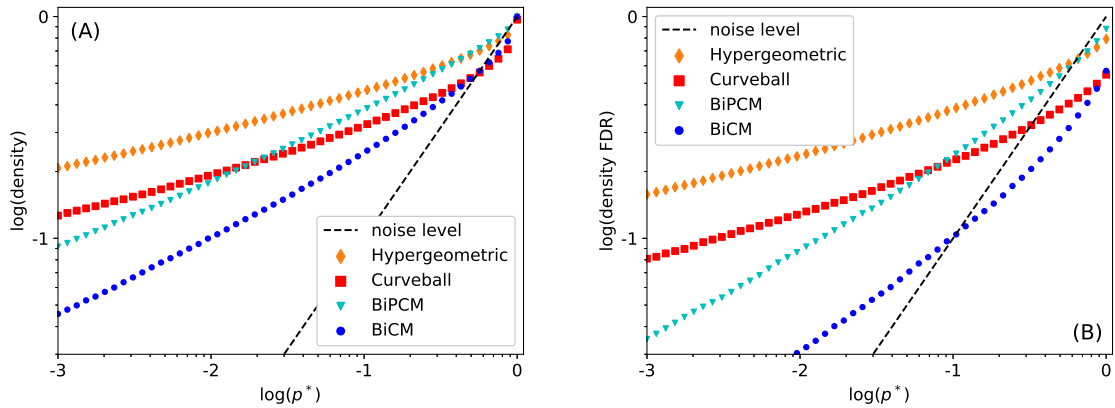
Supplementary Figure 6. Probability distribution of the total co-occurrences S (normalized by their maximum value $S_{max} = |L|^2|\Gamma|$) of a fully connected bipartite network) in the various null model formulations.

SUPPLEMENTARY NOTE 4: CORRECTION FOR MULTIPLE TESTING WITH THE FALSE DISCOVERY RATE

The statistical hypothesis testing procedure described in the main text applies the same significance threshold or confidence level p^* to each test considered individually. Then we vary p^* to compare the various null model outcomes. However we can also consider a correction for p^* in order to obtain a confidence level for the whole family of simultaneous tests. This is a common approach in the literature to minimize Type I errors; in the context of bipartite network projections, it can be appropriate when co-occurrences between the various node pairs cannot be considered independent realization of a generative process (however they still represent different instances).

Here we study whether this correction would have similar effects for the various null models. This is trivially true for the Bonferroni correction, which simply consists in rescaling the threshold p^* by the number of hypothesis tested, namely $m = L(L - 1)/2$ (the same number for all null models). The same outcome is not guaranteed for the False Discovery Rate (FDR) [4], which for a given p^* prescribes to order the observed p-values in ascending order (denoting them by $p^{(1)}, \dots, p^{(m)}$) and validate the k smallest p-values, where k is such that $p^{(k)} \leq kp^*/m$.

Supplementary Figure 7 shows that FDR reduces the number of links that are validated in a similar fashion among the various null models: we do not observe a situation in which the correction is minimal for a null model while for another is more pronounced. Therefore we can conclude that correcting for multiple tests causes a rescaling of the validated network density with respect to p^* , but does not alter qualitatively the results of our analysis.

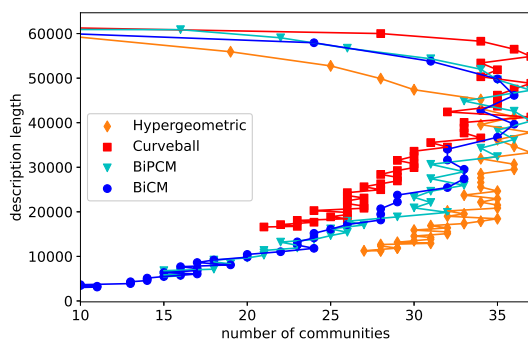


Supplementary Figure 7. Density ρ of links validated by the various null models as a function of the significance threshold p^* , with no correction for multiple tests (panel A) and correction with False Discovery Rate (panel B) applied to all null models.

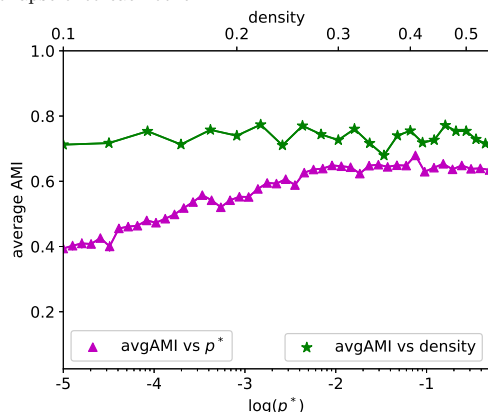
SUPPLEMENTARY NOTE 5: COMMUNITY DETECTION WITH BAYESIAN STOCHASTIC BLOCKMODELING

In this section we check the consistency of our results using a community detection method based on Bayesian inference of the best stochastic blockmodel (SBM) fit of the network [5, 6]. The cost function to minimize in this case is called *description length*, which represents the amount of information needed to describe the network. A detailed description of the method and the accompanying code is available at <https://graph-tool.skewed.de/static/doc/demos/inference/inference.html#the-stochastic-block-model-sbm>.

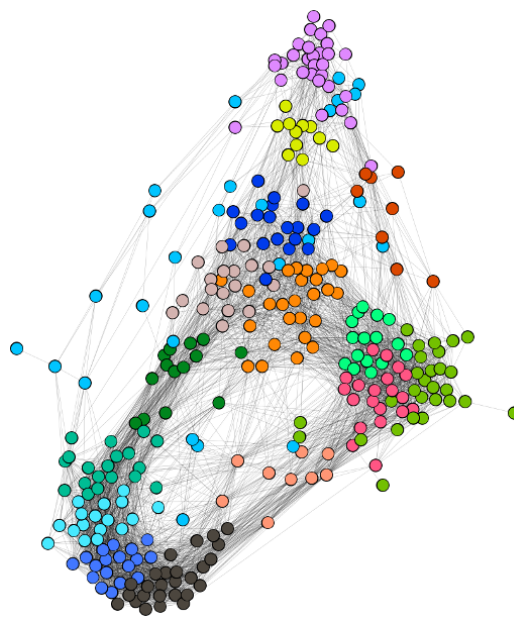
Supplementary Figures 8-10 show that this method leads to a rather different network partition characterized by many more communities. Obtaining different outcomes is common when there is no clear-cut community structure, which is typically the case with empirical applications. However the main point of our work, namely that the various null models can lead to a shared community structure, and that in order to find such meta-structure the validated networks should be compared at identical density values, is still supported by these results.



Supplementary Figure 8. Description length versus number of communities for the best SBM partition obtained on the network validated using the various null models. As in the case of Modularity, also here the curves of the various models collapse onto each other.



Supplementary Figure 9. Average AMI between the best SBM partitions of the network validated by the various null models. Values are plotted for filtered networks obtained with the same p^* (magenta triangles) or of equal density (green stars). The latter option reveals a higher concordance among the null models.



Supplementary Figure 10. SBM-induced community structure for the network of co-occurrence between scientific fields, validated by the BiCM null model for $p^* = 0.0126$ and $\rho = 0.18$ (corresponding to the maximum AMI as of Supplementary Figure 9).

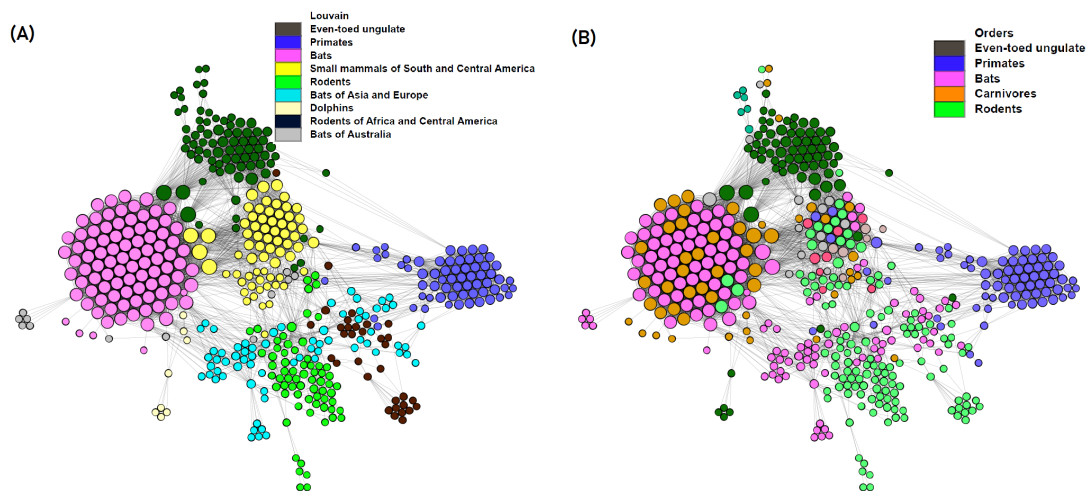
SUPPLEMENTARY NOTE 6: TEST ON BIPARTITE NETWORKS FROM DIFFERENT DOMAINS

To further support the general applicability of our framework, here we report results of the same analysis performed in the main text for several other bipartite networks belonging to totally different contexts². The purpose is to show that our framework can be generalized when the nature of both nodes and links change drastically. We consider:

- *HOST-VIRUS*: a network of 586 viruses, 754 mammalian species, and 2805 relations between mammals and viruses they can host (*i.e.*, be infected by) [7]. We consider co-occurrences between mammals, defined in terms of number of different viruses they can both host. Data available at <https://github.com/cjcarlson/brevity/tree/master/01ival%20Nature%202017%20Raw%20Data>. Results are reported in Supplementary Figure 13.
- *ROBERT* plant: a network of 1429 animal species visiting flowers of 456 plant species that grew in a small area in southwestern Illinois, USA [8]. We consider co-occurrences between plant species, defined in terms of the different animal species they are visited by. Data available at https://iwdb.nceas.ucsb.edu/html/robertson_1929.html. Results are reported in Supplementary Figure 14.
- *TAYLOR* World Cities: a network about the service values (indicating the importance of a city in the office network of a firm) of 100 global service firms distributed across 315 cities worldwide [9]. Data are collected in year 2000; links are weighted according to the service value, ranging from 0 to 5. We thus employed the RCA filter and consider co-occurrences between cities, defined in terms of the different important firms office they host in common. Data available at <http://vlado.fmf.uni-lj.si/pub/networks/data/mix/mixed.htm>. Results are reported in Supplementary Figure 15.
- *DUTCH* elite: a network of 200 persons (corporate elite) who sit on the boards of the 395 most important administrative bodies in The Netherlands [10]. We consider co-occurrences between corporate elites, defined in terms of the different boards they both sit on. Data available at <http://vlado.fmf.uni-lj.si/pub/networks/data/2mode/DutchElite.htm>. Results are reported in Supplementary Figure 16.
- *CRIME*: network of 829 persons and 551 crime cases (collected in 1990s in St. Louis), with link connecting persons to the cases where they appeared as either a suspect, a victim, a witness. We consider co-occurrences between crimes, defined in terms of persons appearing in both. Data available at http://konect.cc/networks/moreno_crime/. Results are reported in Supplementary Figure 17.
- *MOVIELENS*: a network of 1000 users, 1700 movies, and 100000 ratings from users to movies [11] (we consider as actual links only the ratings bigger than 3). We consider co-occurrences between movies, defined in terms of number of different users that rated both of them. Data available at <https://grouplens.org/datasets/movielens/100k/>. Results are reported in Supplementary Figure 18.

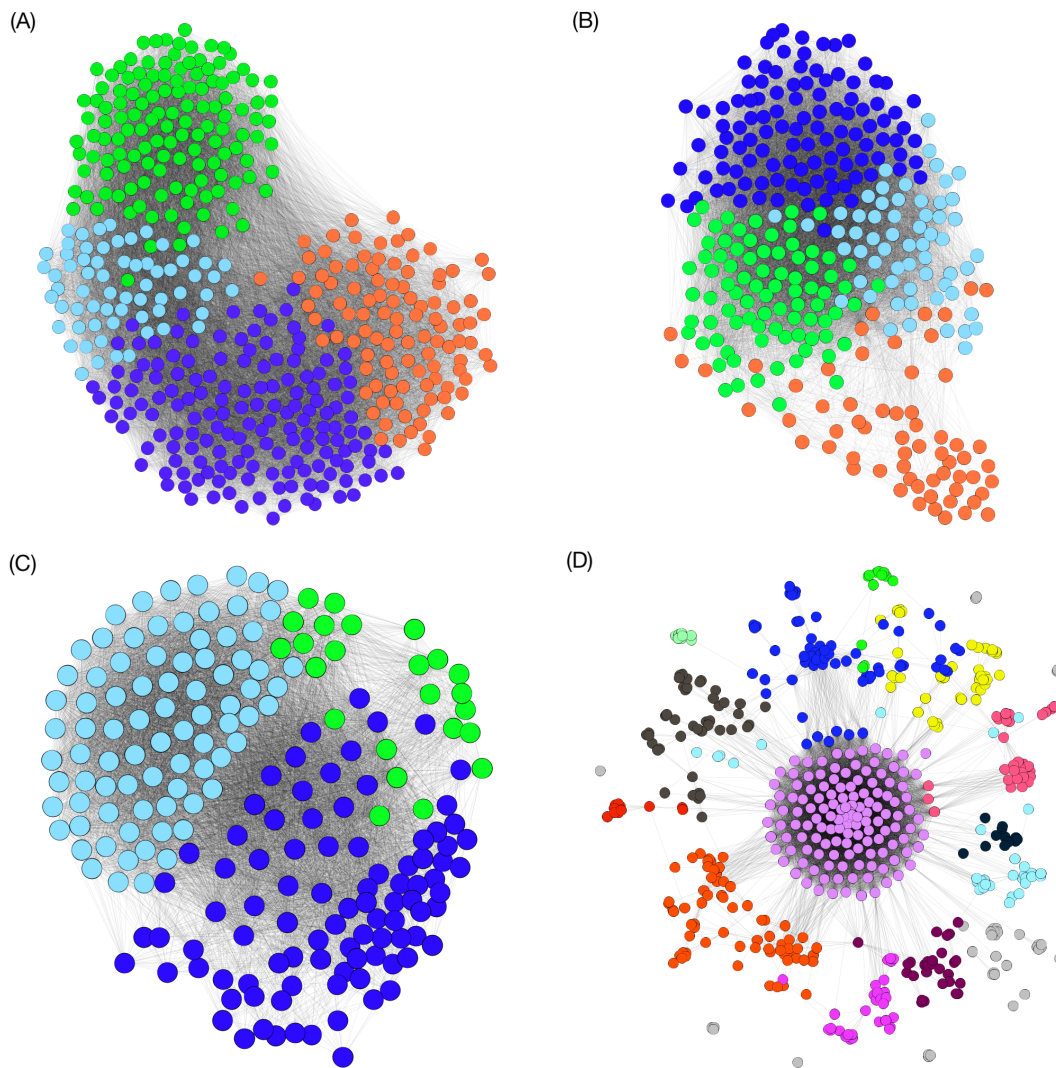
Despite the different nature of these networks, in general we find the same results of the analysis in the main text, namely that the equal-density criterion reveals a consistently higher concordance among the null models. In particular, concerning the community structure, often we can identify a region of “best” agreement between the validation models, indicating which density value (and, as a consequence, which p^*) should be chosen in order to obtain a meta-validated network. This happens when we can find a sufficiently high value of modularity, *i.e.*, when a robust community structure emerges — as in the case of *HOST-VIRUS* (Supplementary Figure 11, where we also compare with metadata-induced partitions) as well as for other networks (Supplementary Figure 12). Otherwise, as in the case of *MOVIELENS*, the AMI values obtained at equal density are not too far from the values obtained at equal p^* , signaling the absence of a community structure in the network.

² Note that we are limited in the choice of dataset that we can use for our exercise for a twofold reason. Firstly, we need a bipartite network with a meaningful modular projection and possibly with metadata. Secondly, in order to include the Curvball algorithm (that relies on numerical sampling) we cannot consider very large systems.

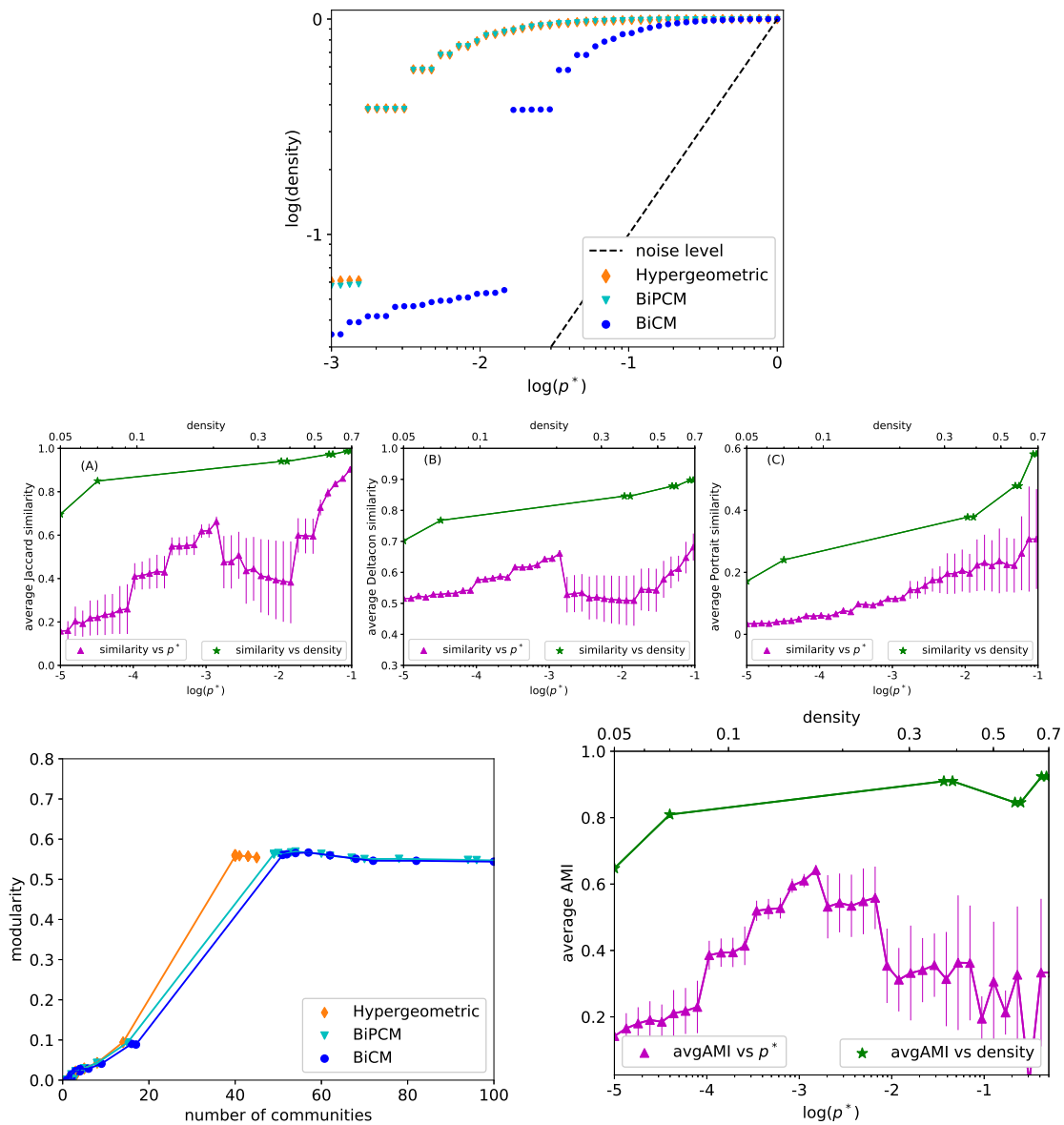


Supplementary Figure 11. *HOST-VIRUS* network: (A) Community structure of the network of co-occurrence between mammalian species (with co-occurrences defined in terms of viruses they can both host), validated by the Hypergeometric null model for $\rho = 0.057$ corresponding to maximum AMI value of the bottom right panel in Supplementary Figure 13. Each color identifies a community (hand-labeled by us as in the legend) shared among the four validated networks. (B) As a comparison, we report the same network with mammalian species labeled according to their species order.

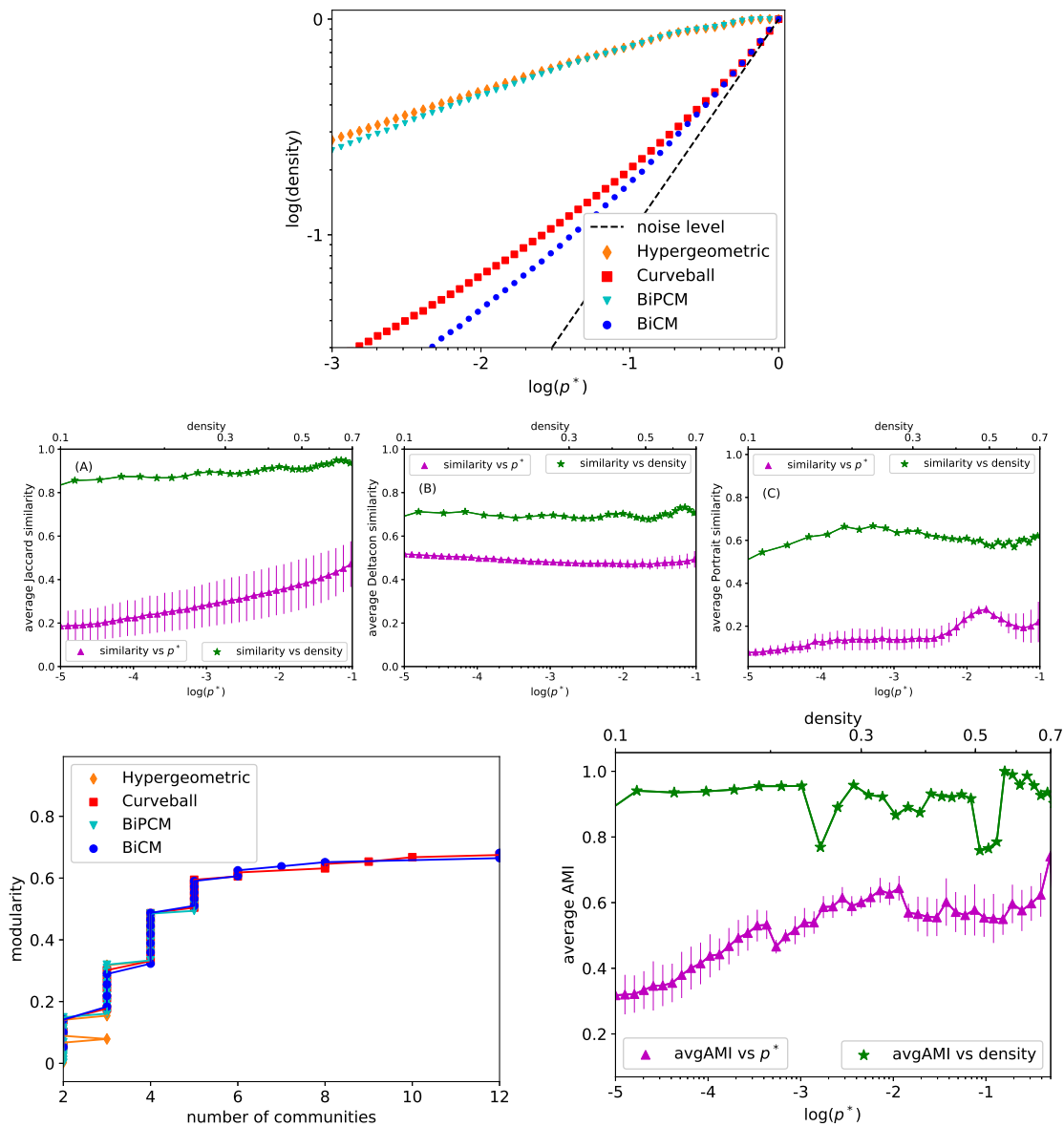
-
- [1] M. A. Serrano, M. Boguñá, and A. Vespignani, Extracting the multiscale backbone of complex weighted networks, *PNAS* **106**, 6483 (2009).
 - [2] D. Garlaschelli and M. I. Loffredo, Generalized bose-fermi statistics and structural correlations in weighted networks, *Physical Review Letters* **102**, 038701 (2009).
 - [3] T. Squartini and D. Garlaschelli, Analytical maximum-likelihood method to detect patterns in real networks, *New Journal of Physics* **13**, 083001 (2011).
 - [4] Y. Benjamini and Y. Hochberg, Controlling the false discovery rate: A practical and powerful approach to multiple testing, *Journal of the Royal Statistical Society. Series B (Methodological)* **57**, 289 (1995).
 - [5] T. P. Peixoto, Efficient monte carlo and greedy heuristic for the inference of stochastic block models, *Physical Review E* **89**, 012804 (2014).
 - [6] T. P. Peixoto, Bayesian stochastic block modeling, in *Advances in Network Clustering and Blockmodeling* (John Wiley & Sons, Ltd, 2019) Chap. 11, pp. 289–332.
 - [7] K. J. Olival, P. R. Hosseini, C. Zambrana-Torrel, N. Ross, T. L. Bogich, and P. Daszak, Host and viral traits predict zoonotic spillover from mammals, *Nature* **546**, 646 (2017).
 - [8] C. Robertson, *Flowers and insects: lists of visitors of four hundred and fifty-three flowers* (Carlinville, Ill., 1977).
 - [9] P. Taylor and B. Derudder, *World City Network: A Global Urban Analysis* (Routledge, 2015).
 - [10] W. de Nooy, Ringen om de macht, in *De elite. De Volkskrant Top 200 van invloedrijkste Nederlanders*, edited by W. Dekker and B. Raaij (Amsterdam, The Netherlands: Meulenhoff, 2006) pp. 85–94.
 - [11] F. M. Harper and J. A. Konstan, The movielens datasets: History and context, *ACM Transactions on Interactive Intelligent Systems* **5**, 1 (2015).



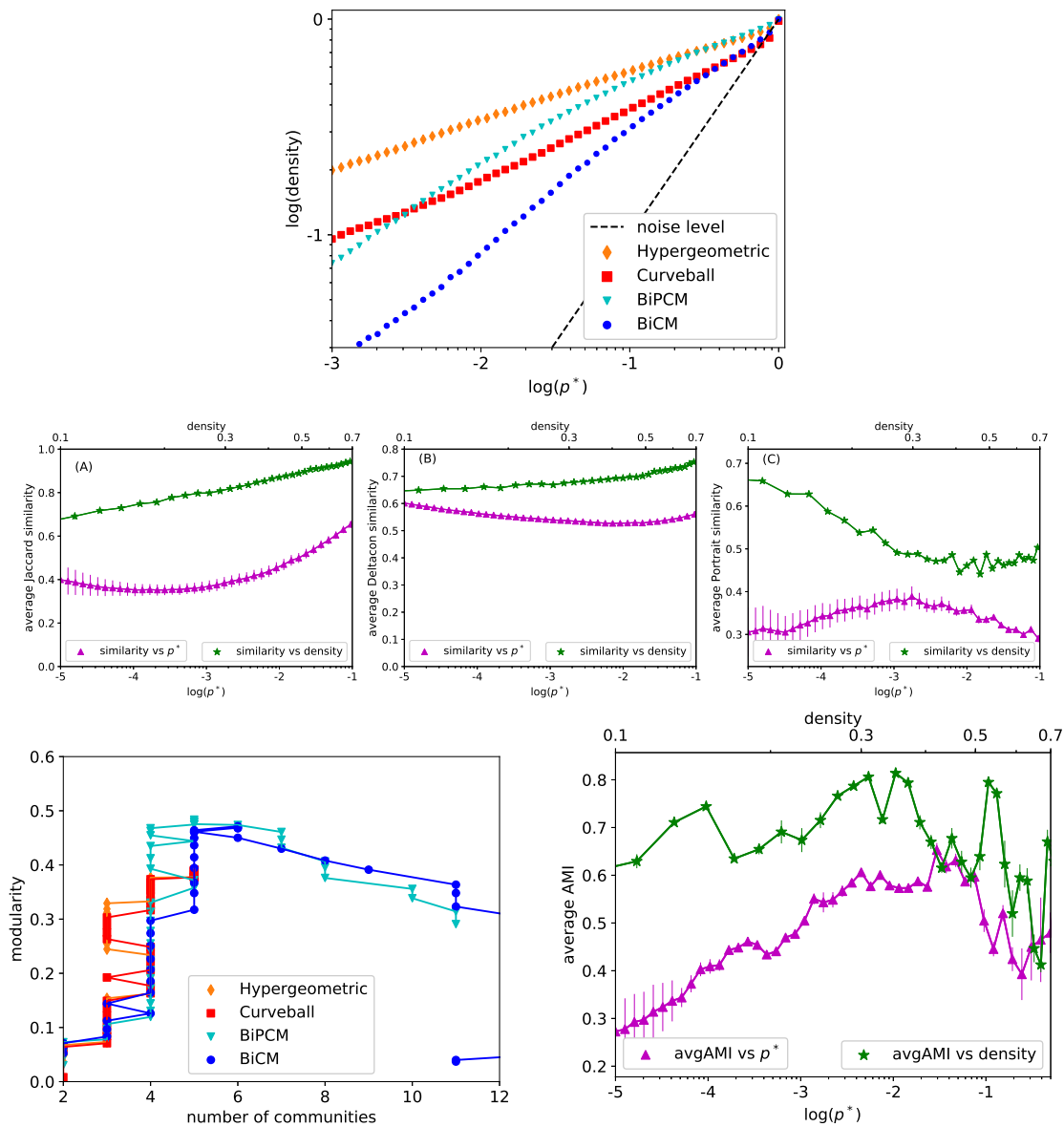
Supplementary Figure 12. Community structures of other networks in our dataset validated by the BiCM null model. Each color identifies a community shared among the four validated networks. (A) *ROBERT* network of co-occurrence between plant species, defined in terms of animal species they are visited by, for $\rho = 0.29$ corresponding to maximum AMI as of Supplementary Figure 14, bottom right panel. (B) *TAYLOR* network of co-occurrence between cities, defined in terms of the different large firms office they host in common, for $\rho = 0.36$ corresponding to maximum AMI as of Supplementary Figure 15, bottom right panel. (C) *DUTCH* network of co-occurrence between corporate elites, defined in terms of the different boards they both sit on, for $\rho = 0.43$ corresponding to maximum AMI as of Supplementary Figure 16, bottom right panel. (D) *CRIME* network of co-occurrence between persons, defined in terms of the different cases they appeared in, for $\rho = 0.08$ corresponding to maximum AMI as of Supplementary Figure 17, bottom right panel.



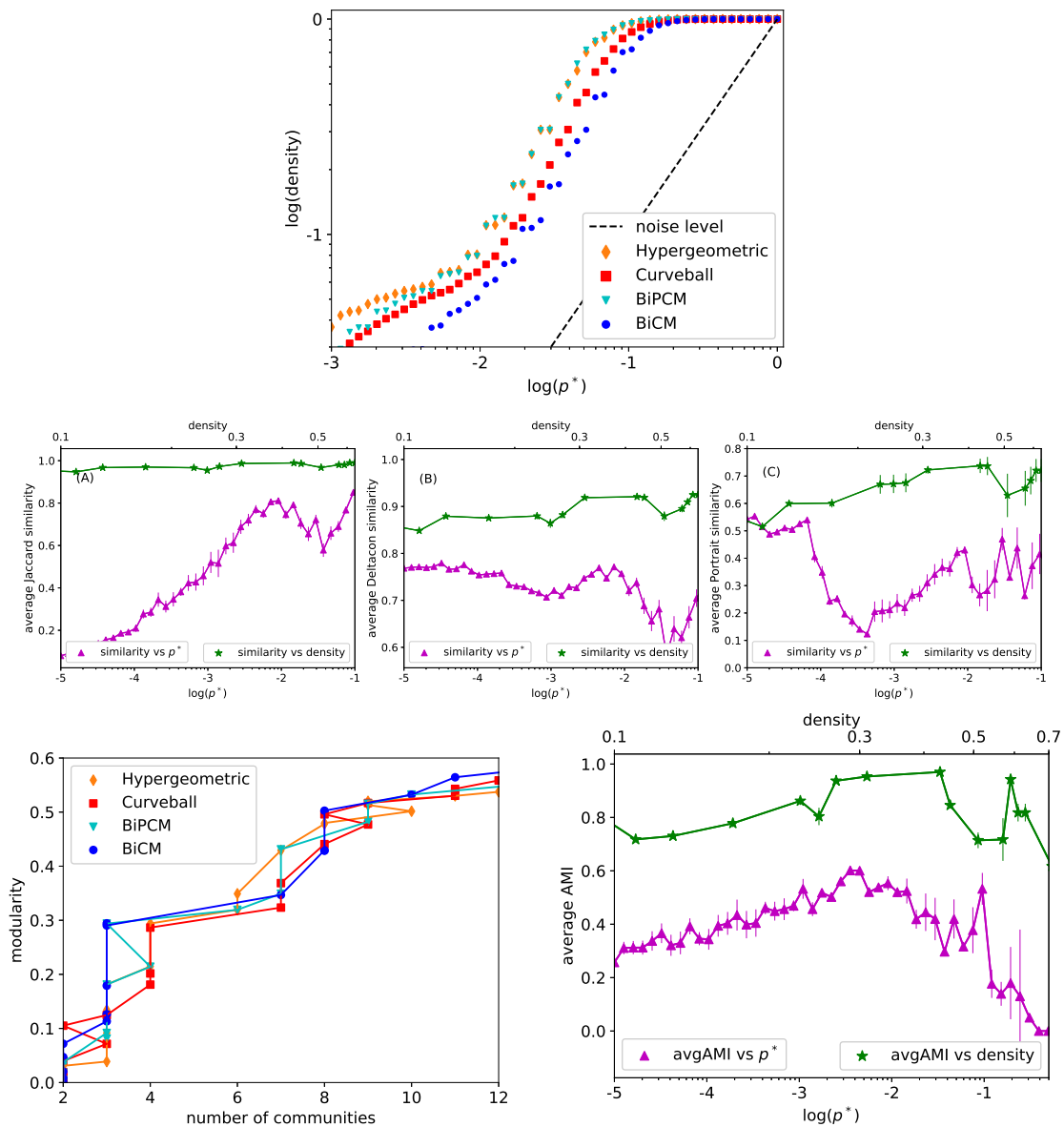
Supplementary Figure 13. *HOST-VIRUS* network. Top panel: density ρ of validated links as a function of p^* . Middle panels: (A) Jaccard, (B) DeltaCon, (C) Portrait similarity of validated networks, as a function of either p^* or ρ . Bottom panels: (left) Modularity vs number of communities; (right) average AMI for partitions of the validated networks as a function of either p^* or ρ . Error bars represent standard deviations over choices of null model pairs.



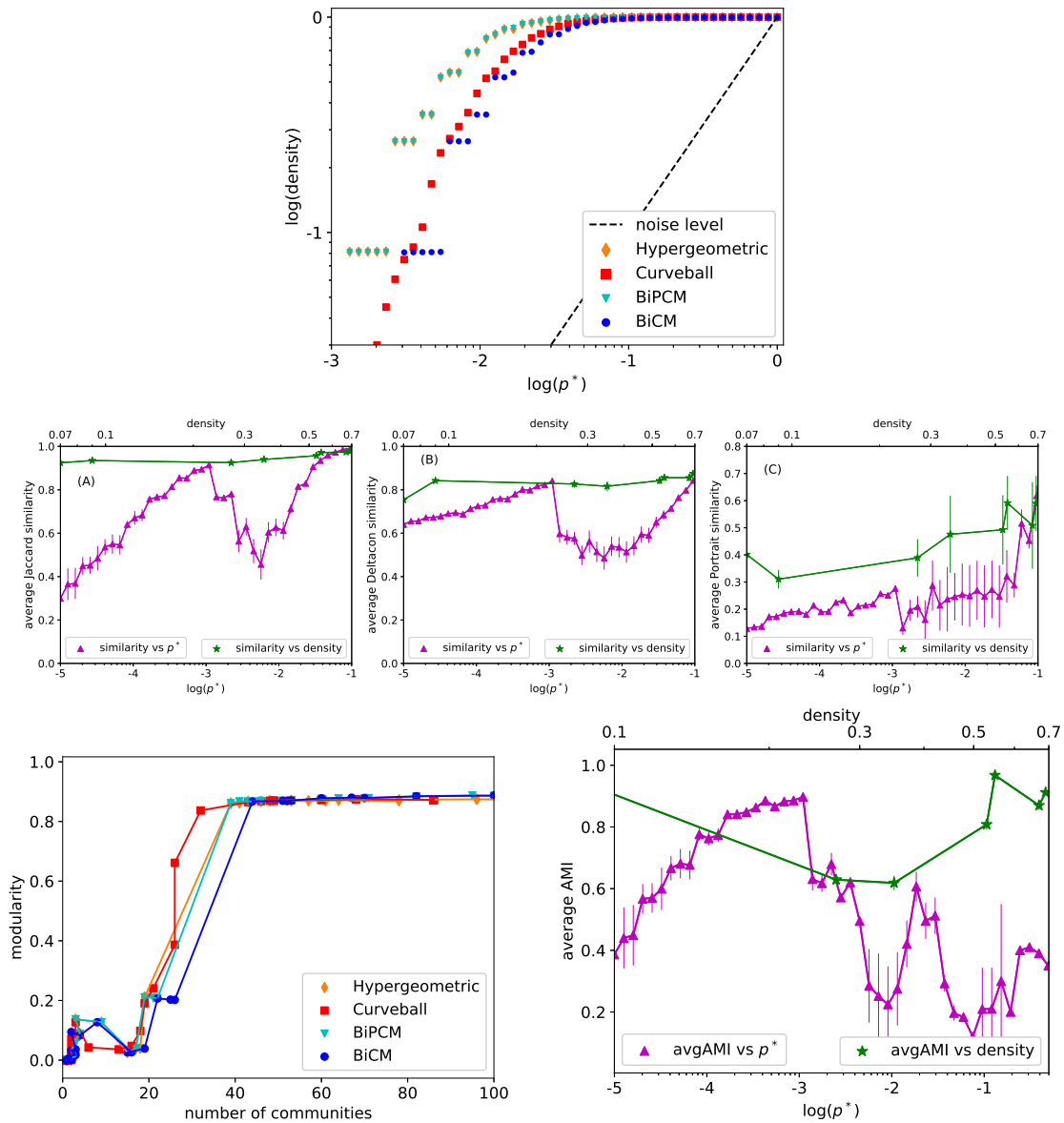
Supplementary Figure 14. *ROBERT* network. Top panel: density ρ of validated links as a function of p^* . Middle panels: (A) Jaccard, (B) DeltaCon, (C) Portrait similarity of validated networks, as a function of either p^* or ρ . Bottom panels: (left) Modularity vs number of communities; (right) average AMI for partitions of the validated networks as a function of either p^* or ρ . Error bars represent standard deviations over choices of null model pairs.



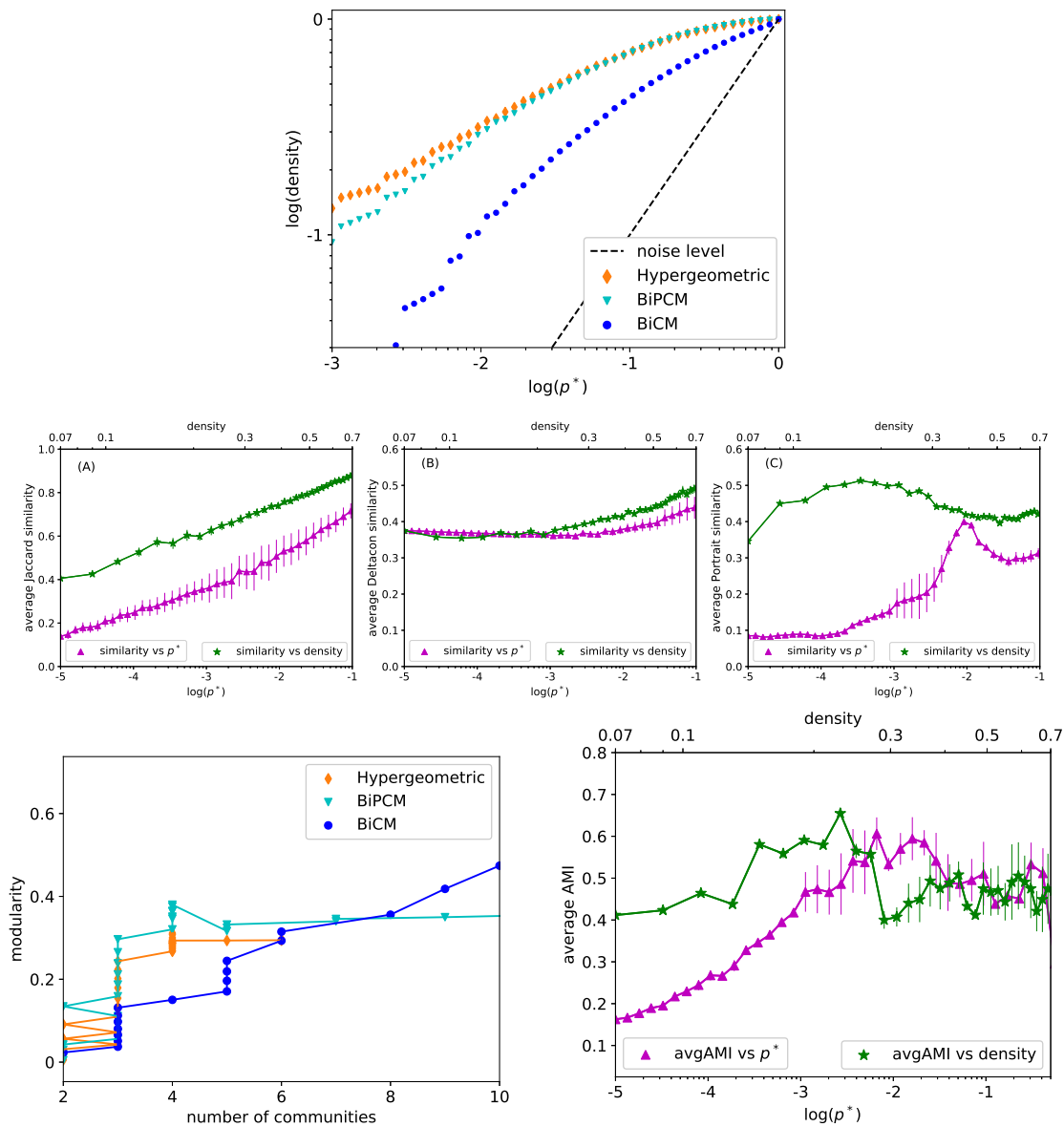
Supplementary Figure 15. *TAYLOR* network. Top panel: density ρ of validated links as a function of p^* . Middle panels: (A) Jaccard, (B) DeltaCon, (C) Portrait similarity of validated networks, as a function of either p^* or ρ . Bottom panels: (left) Modularity vs number of communities; (right) average AMI for partitions of the validated networks as a function of either p^* or ρ . Error bars represent standard deviations over choices of null model pairs.



Supplementary Figure 16. *DUTCH* network. Top panel: density ρ of validated links as a function of p^* . Middle panels: (A) Jaccard, (B) DeltaCon, (C) Portrait similarity of validated networks, as a function of either p^* or ρ . Bottom panels: (left) Modularity vs number of communities; (right) average AMI for partitions of the validated networks as a function of either p^* or ρ . Error bars represent standard deviations over choices of null model pairs.



Supplementary Figure 17. *CRIME* network. Top panel: density ρ of validated links as a function of p^* . Middle panels: (A) Jaccard, (B) DeltaCon, (C) Portrait similarity of validated networks, as a function of either p^* or ρ . Bottom panels: (left) Modularity vs number of communities; (right) average AMI for partitions of the validated networks as a function of either p^* or ρ . Error bars represent standard deviations over choices of null model pairs.



Supplementary Figure 18. *MOVIELENS* network. Top panel: density ρ of validated links as a function of p^* . Middle panels: (A) Jaccard, (B) DeltaCon, (C) Portrait similarity of validated networks, as a function of either p^* or ρ . Bottom panels: (left) Modularity vs number of communities; (right) average AMI for partitions of the validated networks as a function of either p^* or ρ . Error bars represent standard deviations over choices of null model pairs.